

**CORRELATION OF HEMODYNAMIC FORCES
AND ANEURYSM GEOMETRY:
RESULTS OF A THREE-DIMENSIONAL
COMPUTATIONAL FLUID DYNAMICS STUDY**

By

Yie Meng Hoi

August 27 2003

A thesis submitted to the
Faculty of the Graduate School of
State University of New York at Buffalo
in partial fulfillment of the requirements for the degree of

Master of Science

Department of Mechanical and Aerospace Engineering

All rights reserved.

The author hereby grants to University at Buffalo, State University of New York and Department of Mechanical and Aerospace Engineering permission to reproduce and to distribute publicly this paper and electronic copies of this thesis document in whole or in part.

Copyrights by
Yie Meng Hoi
Department of Mechanical and Aerospace Engineering
University at Buffalo, State University of New York
Buffalo, NY
2003

To

MY PARENTS

for

their tireless sacrifice, love, and cheerful encouragement

Acknowledgment

I wish to express my sincere thanks to my advisor, Dr. Hui Meng, for her guidance, advice and support throughout the entire course of research work. Her valuable insights and encouragement have become an impact to my academic life and to this work. My sincere thanks go to the committee members Dr. Dale Taulbee, Dr. Kenneth Hoffmann, and Mr. Scott Woodward for their valuable advice and comments on my thesis. Without them, this work would not be completed.

Special thanks to former and current members of Toshiba Stroke Research Center (TSRC) and Laser Flow Diagnostic Laboratory (LFD): Dr. Benard Bendok, Dr. Ricardo Hanel, Dr. Stephen Rudin, Dr. Balaz Nemes, Dr. Lee R. Guterman, Dr. L. Nelson Hopkins, Stephanie Harvey, Zhijie Wang, Yixiang Feng, Amol Mulay, Dale Hess, Jon Dudley, Minsuok Kim, Dr. Ye Pu, Dr. Gang Pan, and Lujie Cao. Thank you all for encouragements, insights and guidance in my work.

I would like to acknowledge Dr. Ching-shi Liu and Markus Tremmel for their patience and helpful discussions on the technical problems in this work. Special thanks to Alan Walczak for providing the data sets of the patient-specific aneurysm model. Also, I am extremely grateful to all my friends for always being there when I need you. To Guo Xin: I can't thank you enough for your enormous supports. You are wonderful!!

Last but not least, I would like express my sincere thanks to my parents and my brother, for their infinite supports, love, patience and understanding throughout my entire education. Without them, this work would not have been possible.

This research is supported by TSRC, University at Buffalo, SUNY. Computational resources are supported by Center for Computational Research (CCR) and Science and Engineering Node Services (SENS), University at Buffalo, SUNY.

Table of Contents

Acknowledgements	iv
Lists of Figures	viii
Nomenclature	xi
Abstract	xii
Chapter 1 Introduction	1
1.1. Risk Factors and Treatments.....	1
1.2. Hemodynamic Environments.....	2
1.3. Motivation and Objective.....	3
Chapter 2 Mechanics of Blood Vessel	6
2.1. Anatomy of Blood Vessel.....	6
2.2. Pathophysiology of Aneurysm.....	6
2.3. Geometrical Parameters of Intracranial Aneurysm.....	8
2.3.1. <i>Aneurysm Size</i>	8
2.3.2. <i>Aspect Ratio</i>	9
2.3.3. <i>Parent Vessel Curvature</i>	10
2.4. Flow Parameters of Intracranial Aneurysms.....	11

2.4.1. Pulsatility.....	11
2.4.2. Nonlinear arterial wall property.....	11
2.4.3. Non-Newtonian effects.....	12
2.5. Conclusions.....	12
Chapter 3 Computational Methodology.....	13
3.1. Governing Equations.....	13
3.2. Geometrical Parameters.....	14
3.3. Computational Mesh.....	14
3.4. Numerical Simulations.....	15
3.5. Hemodynamic Properties.....	16
Chapter 4 Results.....	20
Chapter 5 Discussions.....	31
5.1. Influence of Elevated WSS on Aneurysm Dilation.....	31
5.2. Risk of Aneurysm Growth Increases with Increasing Arterial Curvature.....	32
5.3. Therapies Developed for Aneurysms on Straight Vessels May Not be Effective for those on Curved Vessels.....	33

5.4. Effectiveness of Endovascular Treatment and Aneurysm Geometry.....	34
Chapter 6 Reconstruction of Patient-Specific Geometry.....	36
6.1. Image Reconstruction Techniques.....	37
6.2. 3D Image Reconstruction from Biplane Angiography.....	38
6.3. Computational Mesh.....	39
6.4. Computational Methodology.....	39
6.5. CFD Analysis.....	40
6.6. Discussions.....	40
6.7. Limitations.....	41
Chapter 7 Conclusions.....	46
Chapter 8 Future Considerations.....	47
Appendix.....	49
Reference.....	53

List of figures

Figure 1.1	Conventional DSA image displays a cerebral aneurysm developed on a curved vessel.....	5
Figure 3.1	Geometrical representation of aneurysm on a curved artery. $1/R$ is the curvature of parent artery, D is the diameter of the aneurysm, N is the major axis of the aneurysm orifice and d is the internal diameter of the parent artery.....	17
Figure 3.2	Computational mesh of aneurysm on curved artery.....	18
Figure 3.3	The assumed waveform that matches a physiological cerebral waveform used in the pulsatile flow simulation.....	19
Figure 4.1	Blood elements paths in model R5 at steady state. Some blood elements never enter the aneurysm whereas others enter the aneurysm from distal end. Of those which entered the aneurysm, some leaves at the distal neck, whereas others join the inflow and whirl irregularly inside the aneurysm.....	23
Figure 4.2	Comparison of velocity field at the symmetry plane of different models at maximum systole. As the arterial degree of curvature increases, flow impingement on the distal neck intensified.....	24

Figure 4.3	WSS distribution at the distal neck of model R5, R4, R1, N2, N3, and N4 at maximum systole of pulsatile flow simulations. The figures shown here are viewed from the Y direction, looking at the distal dome and neck.....	25
Figure 4.4	The size of impact zone at peak systole is a function of aneurysm neck size (N) and curvature (1/R). A larger aneurysm neck size on a more tortuous artery may promote artery remodeling and an increased likelihood of aneurysm growth.....	26
Figure 4.5	With increasing curvature (greater tortuosity), the size of impact zone increases approximately linearly. Higher degrees of arterial curvature or higher flow rate may induce more active arterial remodeling and promote aneurysm growth.....	27
Figure 4.6	The size of impact zone at the distal neck, in which the WSS was greater than 20 dyne/cm ² , changed dynamically during a cardiac cycle. This variation is more pronounced with increasing arterial curvature from model R2 to R6.....	28
Figure 4.7	Velocity vector field in model R1, R2, R4 and R5 at steady state, time-averaged and maximum systole of pulsatile flow simulations. The figures displayed the plane X-X (symmetry plane) of aneurysm.....	29

Figure 4.8	Comparison of velocity profile and WSS distribution of model R6 a,c) steady state simulation with Re equal to maximum systole in pulsatile flow, and b,d) pulsatile simulation at maximum systole.....	30
Figure 6.1	A patient-specific procedure framework to facilitate physicians to make scientifically sound clinical decisions.....	37
Figure 6.2	A patient-specific aneurysm model from angiography.....	43
Figure 6.3	The computational mesh of patient-specific aneurysm geometry.....	44
Figure 6.4	The CFD simulation of blood particle paths in patient-specific aneurysm.....	45

Nomenclatures

D	Maximum aneurysm diameter
d	Internal arterial diameter
N	Aneurysm neck size (Major axis of aneurysm orifice)
P	Pressure (Pa)
R	Radius of arterial curvature (mm)
Re	Reynolds number
U	Velocity (m/s)
WSS	Wall shear stress (dyne/cm ²)
μ	Viscosity of fluid (cP)
ρ	Density of fluid (kg/m ³)

Abstract

The objective of this study was to investigate the effects of arterial curvature and aneurysm neck size on aneurysmal hemodynamics and assess implications relative to aneurysm on the growth and treatment effectiveness of these aneurysms. The hemodynamics of three-dimensional (3D) lateral aneurysms on arteries of ten different sets of arterial curvature were studied using computational fluid dynamic (CFD) analysis. Both steady and pulsatile flow simulations were conducted. The effects of these geometric parameters on hemodynamic parameters including flow velocity, aneurysm wall shear stress (WSS), and area of highest WSS elevation measured during the cardiac cycle (the time-dependent impact zone) were quantified. Unlike in simulations involving aneurysms located on straight arteries, blood flow inertia (centrifugal effects), rather than the viscous diffusion, was the predominant force driving flow into the sacs of aneurysms on curved arteries. As the degree of arterial curvature increased, flow impingement on the distal neck intensified, which led to elevations in pressure, WSS and enlargement of the impact zone at the distal neck. The large impact zone on the aneurysm distal neck and wall implicates this area as the most likely site of aneurysm initiation, growth or regrowth of a treated aneurysm. Thus, lateral aneurysms on more tortuous arteries have a greater tendency of continued growth. Moreover, lateral aneurysms with wide neck on a tortuous vessel should be treated with greater urgency. The protection of the aneurysm distal neck from flow impingement is critical to prevent further aneurysm growth or regrowth. Finally, CFD and medical images were integrated to provide more insights on the pathophysiology of aneurysm.

Chapter 1 Introduction

Stroke, as a result of insufficient blood flow to the brain, causes brain injury. It is the third leading cause of death in North America [1]. Stroke killed 158,448 people (61.4% among women) in 1998 and accounted for about 1 in 15 deaths in the United States [1]. Approximately 7% of stroke is caused by subarachnoid hemorrhage (SAH).[2] SAH is volumetric filling of blood into the area surrounding the brain, resultant compression of the tissues and vessels, leads to permanent disability, brain damage or death. There are 90% of all SAH cases come from aneurysm rupture [2].

An aneurysm is a local dilation of a blood vessel that poses a risk to health from rupture, clotting, or dissecting. Despite latest endovascular interventions and techniques, the mortality and morbidity aneurysm remain very high. Approximately 50% of patients with aneurysmal SAH will die or suffer permanently disability, such as loss of speech, memory lapses or paralyzed. Another 23%-35% will die due to subsequent hemorrhages if left untreated [3] and 15% of the patients will die before reaching the hospital. The majority of the patients are at the age of 35-60, with slightly higher rate of occurrence in woman.

1.1. Risk Factors and Treatments

Clinical studies have indicated that smoking, excessive use of alcohol and hypertension are the major risk factors in aneurysm formation. In addition, patients who suffer from atherosclerosis, traumatic head injury or family member with stroke history are also in the high-risk groups. Although the cause of aneurysm initiation, growth and rupture remains ambiguity, it is widely accepted that the blood flow dynamic is closely related to the pathogenesis of this type of vascular disease.

Currently, there are two types of surgical procedures to treat an aneurysm, i.e. surgical clipping and endovascular treatments. The surgical clipping involves opening of skull, identifying the aneurysm, and inserting a metallic clips at the aneurysm neck to prevent the blood from entering the aneurysm. Surgical clipping is a high risk, invasive procedure and it is usually not recommended for senior patients. Endovascular procedure involves deploying coils or injecting liquid emboli into the aneurysm cavity to block the blood from entering the aneurysm. It is less invasive; but the success of these treatments remains ambiguous due to aneurysm regrowth, coil compaction or spontaneous rupture. Due to the asymptomatic nature of the disease, there is no effective diagnostic and treatment available for the patients currently.

The integrations of biological factors and biophysical forces have increased the complexity of the aneurysm genesis, growth and rupture. [4] More importantly, the treatments of aneurysm remain at high mortality and morbidity due to insufficient understanding of the interaction among blood flow, vessel wall and intervention designs. Thus, to improve the diagnostic and to increase durability of aneurysm treatment, the physiological behaviors of blood flow in the diseased artery have to be acknowledged.

1.2. Hemodynamic Environment

Hemodynamics can be defined as the study of blood flow and the physical forces concerned in the circulatory system. Although patients' genetic, anatomic, histological, and physiological factors have been implicated in the pathogenesis of aneurysm, the hemodynamic forces play significant roles in the development and progression of aneurysm.

As blood flows in the vessel, the luminal surface of the blood vessel and the endothelial cells are constantly exposed to different level of hemodynamic shear stress. [5]

In numerous experiments, shear stress has been shown to actively influence vessel wall remodeling. [6, 7, 44, 88] The wall shear stress (WSS) is proportional to the velocity gradient at the wall and the fluid viscosity (μ):

$$WSS = \mu \left. \frac{\partial u}{\partial y} \right|_{y @ wall} \quad \text{(Equation 1.1)}$$

Arteries adapt to long-term increases or decreases in wall shear stress. The response to increased wall shear stress is to vasodilate and then remodel to a larger diameter with the same arterial structure. Conversely, decreased shear stress resulting from lower flow induces vasoconstriction and remodel to decrease in internal vessel radius. [8] The responses of arteries to the different hemodynamic environment may constitute to the normal adaptation or pathological disease. [90]

1.3. Motivation and Objective

In vivo observations have verified that lateral aneurysms have significant tendency to be induced at vessel bifurcations and curves (Figure 1.1) [40]. The anatomically localized aneurysm formation strongly implicates the relationship between the hemodynamic forces and arterial geometry in the disease process. [9] Several authors have performed experimental and statistical analysis on aneurysm size, or aneurysm aspect ratio to assess the risk of aneurysm rupture. [33-38] However, these proposed geometrical parameters failed to address the pathological process of aneurysm. The statistical analysis is population dependent and cannot be freely applied to the group outside the study population. In an attempt to understand the initiation, growth and rupture of aneurysm, aneurysm located on straight vessel model is frequently used. [32] Nevertheless, aneurysm located on a straight segment of an artery is rarely observed in the clinical cases. Furthermore, the two-

dimensional aneurysm model is over-simplified and inadequate to mimic the physiological hemodynamic environment. [37, 47]

This study focused on three-dimensional (3D) generic idealized aneurysm geometry, which elucidated the importance of arterial curvature and aneurysm neck size through computational fluid dynamic (CFD) analysis. The model of aneurysm located on curved artery is closer to clinical observations, and is more complex than the previous sidewall aneurysm models. A better understanding of the relationship between aneurysm pathophysiology and artery geometry is needed to understand aneurysm growth, predict the risk of aneurysm regrowth and to design appropriate treatments. Utilizing the flexibility of CFD analysis, the hemodynamic of aneurysm, with different neck size, located on different curved vessels were investigated. In addition, this study also explored the techniques to integrate CFD analysis and medical images to investigate the hemodynamic of anatomically realistic aneurysm model. The techniques will provide crucial evolution to study the vascular disease, predict the outcome of interventional procedures, and aid the clinicians to decide the best treatment for individual patients.

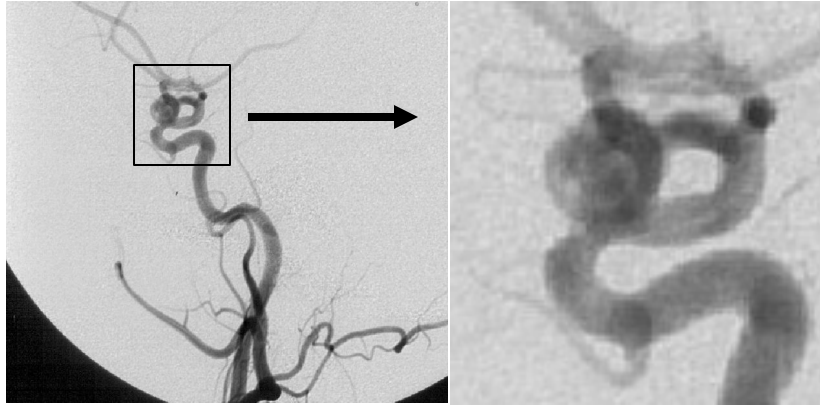


Figure 1.1: Conventional DSA image displays a cerebral aneurysm developed on a curved vessel.

Chapter 2 Mechanics of Blood Vessel

2.1. Anatomy of Blood Vessel

The walls of blood vessel consist of similar structures but inhomogeneous components. [10, 11] The arteries consist of three distinct material layers, i.e. tunica intima, tunica media and tunica adventitia. The intima is the innermost layer of the vessel. It consists of a monolayer of endothelial linings ($\sim 0.05\text{-}0.1\ \mu\text{m}$) in contact with flowing blood. [12] The endothelial cells play important roles in regulating the vessel response to the change of blood flow. The media is organized into alternating layers of interconnected smooth muscle cells and elastic lamellae, with rich elastin and collagen. The smooth-muscle cells proliferate to change the mechanical characteristics of the wall. Both smooth muscle cells and the elastic lamellae provide the mechanical strength to the vessel to sustain structural integrity. The adventitia merges externally with surrounding tissue and consists of high proportion of collagen, and loose, more disorganized fibrous connective tissue. [12]

2.2. Pathophysiology of Aneurysm

Blood vessels undergo remodeling when the hemodynamic forces imposed on them are altered. This remodeling process influences vascular development, long-term adaptation and the progression of vascular diseases such as atherosclerosis and aneurysm formation. [62, 63, 90]

Aneurysm formation has been widely accepted as degenerative vascular lesions. [24] The aneurysm wall is thin, consists of mainly collagen and small amount of elastin and smooth muscle layers. [25-27, 36] Due to its asymptomatic nature and lack of animal models, the mechanism of how the vasculature degenerates to form an aneurysm remains

unclear. Nevertheless, several studies have been attempted to understand the aneurysm pathogenesis.

Genetic factors have been implicated to the pathogenesis of aneurysms as evidenced by familial cases of aneurysms. [120] Nevertheless, the study of aneurysm genesis based on genetic factor is statistically insignificant to correlate aneurysm formation and genetic diseases.

Hypertension has been correlated to the abnormal amount of elastin and collagen in the arterial wall. [56, 57] The degenerated elastin and collagen, especially Type III collagen, suggests remodeling process of the extracellular matrix. [118, 119] The altered matrix composition weakens the vessel wall, and becomes less resistant to the incessant flow impingement and high pressure, resulting in arterial dilation and aneurysm formation. [56] However, given the degeneration of elastin and collagen, the possibility of regeneration of elastin and collagen to restore the mechanical strength of artery wall is still under investigation.

Flow-induced hemodynamic stresses have been emphasized in the formation, growth and rupture of aneurysm. [4, 24, 28] The vessel geometry near branches, bifurcations, flow divider, and curved regions promotes flow impingement, flow separation, high/low WSS distribution and vortex formation. [42, 43, 112] As a result, the structural and functional properties of the wall are changed to adapt the altered hemodynamic environment. [34, 102] At the innermost of the arterial wall, the endothelium functions as mechanical sensitive signal transduction interface between the blood and arterial wall. [5, 112] *In vivo* experiments supported the theory that aneurysm initiation is a degenerative process in the endothelium around the apex due to increased WSS. [70, 110] The endothelial cells respond to the elevated WSS by releasing vasodilation factors, including nitric oxide (NO),

prostacyclin (PGI₂), and matrix metalloproteinases (MMP), to dilate the wall in an attempt to return the WSS to physiological baseline levels. [60-66] The increased levels of MMP and NO are capable of weakening the vascular integrity. [51-55] In addition, the intra-aneurysmal pressure is directly responsible for the circumferential stretching of the degraded wall, resulting in enlargement of the dome and eventual rupture. [71] The vascular structural changes cause the focal weakening in the arterial wall, resulting in bulging and forming an aneurysm. [56]

Despite numerous efforts to understand the pathogenesis of aneurysm, the fact that aneurysms are most frequently found at the bifurcation and curved sections of the cerebral arteries strongly implicates the relationship between the hemodynamic forces and arterial geometry in the disease process. [9] The hemodynamic forces are characterized by the local arterial geometries, which then affect the wall structure through flow-induced shear stress. [34, 102] Thus, the local aneurysm geometry is the central to hemodynamic forces.

2.3. Geometrical Parameters of Intracranial Aneurysms

The geometrical parameters have been widely used to identify the category and characteristic of aneurysms for making treatment decisions. Without the clear understanding of how these geometrical parameters influence the pathogenesis and the treatment of aneurysm, the geometrical parameters are inadequate to draw a concrete suggestion in making treatment decisions. Nevertheless, these parameters include:

2.3.1. Aneurysm Size

Many researches have attempted to determine whether there is a critical size at which an aneurysm is likely to rupture. [50] Members of the Stroke Council concluded that incidental aneurysms smaller than 10mm should be observed rather than treated. [19] In a

study conducted by Rosenorn et al., among the 908 ruptured aneurysms that had a maximum diameter less than 25 mm, 162 ruptured aneurysms were less than 5 mm, 474 and 272 were between 5-10 mm and 11-24 mm, respectively. [20, 21] They recommended that unruptured aneurysms with a size 10 mm or less should be seriously considered for operative closure of the aneurysm. Kassel et al. suggested aneurysm greater than 5mm in diameter were hazardous and treatment should be considered immediately, whereas Crompton suggested the critical size at which an aneurysm is about to rupture is between 2 and 5mm. [35, 36] However, a lot of clinical reports revealed that aneurysm can rupture at smaller than 5mm or remain unruptured at greater than 10mm. [19-21, 49, 50, 106, 107] In vitro experiment showed that as the aneurysm size increases, the inflow angle to the aneurysm decreases, thereby reducing the flow activity in the aneurysm. [58, 59] Thus, the aneurysm becomes more susceptible to thrombosis. It is, therefore, possible that large aneurysm remains unruptured. Consequently, although there is a critical size for the rupture of each aneurysm, it is quite unlikely that this size is identical in each aneurysm. [41] Thus, the risk assessment based on aneurysm size alone is insufficient to predict the outcome of aneurysm therapy.

2.3.2. *Aspect Ratio*

The characteristic of aneurysm neck and size defines the volume and velocity of flow into and out of the aneurysm, thereby affects the distribution of hemodynamic stresses. [33] Thus, Ujiie *et al.* defined the geometrical parameter, aspect ratio as the ratio of aneurysm depth to aneurysm neck width. [33, 34] This parameter includes the aneurysm neck width in addition to the aneurysm size alone. Ujiie *et al.* showed that 80% of all aneurysms with aspect ratio of 1.6 or higher were ruptured aneurysms. [33, 34] The difference in aspect ratios between the ruptured aneurysm and unruptured aneurysms was statistically significant. [34] However, in the same study, 20% of ruptured aneurysms are associated with aspect ratio less than 1.6, which cannot be excluded from treatment.

Nevertheless, Ujiie et al. have shown that the aneurysm geometry is important to address the development and risks. The development of aneurysm into non-spherical shape, as seen in clinical cases, is intuitively relevant to the hemodynamic stresses.

2.3.3. *Parent Vessel Curvature*

Aneurysms are frequently discovered on curved arteries in clinical cases suggesting that the hemodynamics in curved arteries may favor the development of aneurysm than straight arteries. More interestingly, most aneurysms are formed at the outer wall, instead of the inner wall of artery. [24, 39, 61] This further indicates that the biological response and the hemodynamic stresses associated with vessel geometry are intuitively relevant, but has not been well-addressed.

In a curved artery, there exists a pressure gradient between the inner wall and outer wall to make the flow turn along the curve. This pressure gradient increases gradually with increasing degree of arterial curvature. The difference between the inner and outer wall pressure gradient generates the centrifugal force. Thus, the velocity profile in the vessel is skewed toward the outer wall, creating a WSS which is lower at the inner wall than at the outer wall. The endothelium at the outer wall will adapt to the altered hemodynamic environment. *In vitro* Particle Tracking Velocimetry experiments found that the aneurysmal inflow velocity, angle, and WSS increase with increasing parent vessel curvature. [58] The hemodynamic stresses resulting from the flow impingement at the curved arterial segment or at the apex of intracranial bifurcation could be an important factor in the focal degeneration of internal elastic membrane leading to aneurysm formation. [23, 29, 39, 47]

The pathophysiology of aneurysm is closely related to the local hemodynamic stresses. These studies of aneurysm geometry are over simplified and insufficient to improve the outcome of therapy. More importantly, these studies fail to correlate the biological

response and the aneurysm geometry. The current study using 3D CFD simulations will provide more accurate understandings than the previous studies. In addition, the CFD results will be correlated with the biological response and clinical observations.

2.4. Flow Parameters of Intracranial Aneurysms

Besides the geometrical factors, the following flow parameters also associate with the magnitude and distribution of hemodynamic stresses.

2.4.1. Pulsatility

Flow instabilities are enhanced with pulsatile flow because of more prominent influences of the inertia of the fluid. [] With unsteady flow in arterial curvature and bifurcation sites, there are regions in which the flow is reversed during part of the cardiac cycle. Hence the WSS varies from a large magnitude in one direction to negative values during part of the cardiac cycle. [90] Fukushima et al. compared steady and unsteady aneurysm flow using experiments and simulations. [13] They found that the pulsatile flow produced a flow pattern which was different from steady flow. Both *in vivo* and *in vitro* experiments discovered that increase in flow rate or pulsatility favors the initiation and growth of aneurysms. [109, 110] Therefore, to mimic the physiological hemodynamic condition and to precisely predict the outcome of treatment, pulsatile flow simulation is adopted in this study.

2.4.2. Nonlinear Arterial Wall Property

As the blood flows through the vessel, the mechanical stresses acting on a vessel is comprised of three components: transmural pressure acting normal to the surface, viscous shear stress acting tangential to the surface, and cyclic elongation in the radial direction. [14] Under these loadings, the vessel substantially displays a more complex response than the

isotropic material stress-strain relationship. The arteries experience 6-10% diameter variation over a cardiac cycle driven by pressure pulse.[15, 16] Arteries, such as aorta, carotid and iliac arteries, consist of thick muscle layers and may be regarded as elastic structures, whereas cerebral arteries, typically display viscoelastic behavior. [12, 14] The interaction between the distensible arterial wall and the flowing blood influences the force pattern on endothelial cells. [17] However, *in vivo* measurement of arterial wall properties is very difficult. The arterial wall properties may vary significantly in the healthy vessel and diseased vessel. The integration of nonlinear vessel wall properties and blood flow dynamics is too complicated and time consuming. Thus, rigid wall model is assumed in this study.

2.4.3. *Non-Newtonian effects*

Blood behaves as non-Newtonian fluid, i.e. the viscosity decreases with increasing shear rate. This non-Newtonian effect becomes more significant in small diameter vessels (<0.1mm) and low shear rate (< 100 s⁻¹). [9, 41] In the large vessels, the viscosity of blood is approximately 3.5cP. [32] Perktold et al. compared the Newtonian effect and non-Newtonian effect in aneurysmal flow and discovered there was no significance difference in their results [18]. Thus, the Newtonian blood property is assumed in this study.

2.5. Conclusions

To predict the outcome of aneurysm treatment or to recommend treatment solutions, we need a clear understanding of how the hemodynamic stresses are affected by the geometrical factors. It is, therefore, very crucial to correlate the relationships between different geometrical parameters and hemodynamic stresses, thereby predict the biological response of the vascular components. In this study, the hemodynamic stresses of more complex and realistic aneurysm geometries were investigated using CFD. These stresses were correlated to the biological response of the vascular components.

Chapter 3 Computational Methodology

Computational fluid dynamics (CFD) has proven to be a reliable tool for studying the arterial flow dynamics. The 3D, complex arterial geometry is discretized into small computational cells using tetrahedral and hexagonal elements. By applying the steady-state or time-dependent boundary conditions, the governing Navier-Stokes equations in each computational cell can be solved to obtain the entire flow field. In addition, other hemodynamic parameters, such as WSS, pressure, residence time, wall deformation, vorticity, and etc, can be accurately derived from the solution.

3.1. Governing Equations

The governing equations that describe the aneurysmal flow are the conservation of mass and conservation of momentum:

Conservation of Mass:
$$\frac{\partial u_i}{\partial x_i} = 0 \tag{Equation 3.1}$$

Conservation of Momentum:
$$\rho \frac{\partial u_i}{\partial t} + \rho u_j \frac{\partial u_i}{\partial x_j} = - \frac{\partial P}{\partial x_i} + \mu \frac{\partial^2 u_i}{\partial x_j^2} \tag{Equation 3.2}$$

Where $x_{i,j}$ ($i,j = 1,2,3$) is the orthotropic directions, u_i is the velocity, t is time, P is pressure, ρ is the density of the fluid, and μ is the viscosity of blood. In this study, the viscosity and density of blood were assumed constant. The body force was neglected in this study since it has comparable small effects on the flow.

3.2. Geometrical Parameters

To isolate the arterial curvature and aneurysm neck size from a host of other geometric and physiological factors presented in patient anatomical aneurysms, idealized aneurysm geometries were adopted in which the parent vessel curvature and aneurysm neck can be systematically varied while keeping other parameters unchanged.

To understand the impact of arterial curvature on hemodynamic forces, 10 lateral aneurysm models are constructed for the computational studies. R is defined as the radius of curvature of the parent artery. The inverse, $1/R$, is known as the curvature. D is the diameter of the aneurysm, N is the width (major axis) of the aneurysm necks and d is the internal diameter of the parent artery (Figure 3.1). In the first group of models, denoted R1 to R6, the geometric variables were kept constant except for arterial curvature ($1/R$) of the parent artery. In the second group of models, denoted N1 to N4, the geometrical variables were kept constant except for the aneurysm neck size (N). In all models, the parent artery was 3 mm in diameter, and the aneurysm was 12 mm in diameter. In the first group, the curvature ranged from 0 to 0.1667mm^{-1} and N was kept at 7.5mm. In the second group, the aneurysm neck size ranged from 6 mm to 9.56 mm, and $1/R$ was fixed at 0.0833mm^{-1} .

3.3. Computational Mesh

The 3D aneurysm models were generated in Pro-Engineer® (PTC, Liverpool, NY). This advanced solid modeling program allows precise control of dimensions and flexibility in generating the models. Once the 3D models were generated, these solid models were imported into Gambit® (Fluent, Lebanon NY) for mesh generation. Gambit® is an automated mesh generation program which supports structured and unstructured meshes.

The boundary layers in each model were first generated in Gambit®. Then, the faces of each model were meshed accordingly using quadrilateral mesh. Finally, the entire solid model was meshed using 3D hybrid tetrahedral and hexagonal mesh. Each 3D model consisted of approximately 500,000 cells (Figure 3.2).

3.4. Numerical Simulations

The finite volume commercial code, STARCD® (Adapco, NY) was used to simulate the 3D blood flow. The mesh which was generated in Gambit® was imported into STARCD. To begin with, the flow properties were first defined in STARCD®. Then, inlet and outlet of the computational domains were selected. Before the simulation, a fully-developed velocity profile was applied to the inlet whereas zero pressure gradients were enforced at the outlet of the computational domains.

Implicit scheme was chosen for the computations since it is unconditionally stable with larger computational time steps. The steady-state flow simulations terminated when user-defined tolerance ($1e-5$) was achieved. In pulsatile flow simulation, the assumed waveform that matches a physiological cerebral waveform used in the pulsatile flow simulation is shown in Figure 3.3. This waveform corresponds to 60bpm was constructed using 4 terms of the Fourier series. The peak systole occurred at 1/3 of the entire cardiac cycle. The computed results from first and second cycle were discarded in order to reduce numerical instability at the beginning of the simulation. The incremental time step was 0.001 seconds. The numerical results were output at every 0.025 seconds.

3.5. Hemodynamic Properties

It is widely accepted that the artery remodels to adapt to the changes in blood flow conditions. WSS is the tangential force exerted by the flowing blood on the luminal surface that retards the flow of blood. The endothelial cells sense mechanical strain caused by elevated WSS and respond to it with a biological response that adjusts the vessel diameter to restore the WSS to a baseline level of 15 to 20 dynes/cm². [44, 45, 67, 104] This is accomplished primarily by the release of vasodilators that allow smooth muscle cells to relax, ultimately causing the vessel dilation. [60-66, 90] Building on this premise, the *area* on the aneurysm walls where the WSS was elevated and greater than 20 dynes/cm², was calculated. This elevated WSS *area* may indicate the active wall remodeling zone on the aneurysm wall. This *area* is defined as the *impact zone*. Blood flow velocity, pressure, and WSS distribution were computed for all aneurysm models through both steady-state and pulsatile flow simulations. In the pulsatile flow simulations, the time-dependent WSS distributions were also computed.

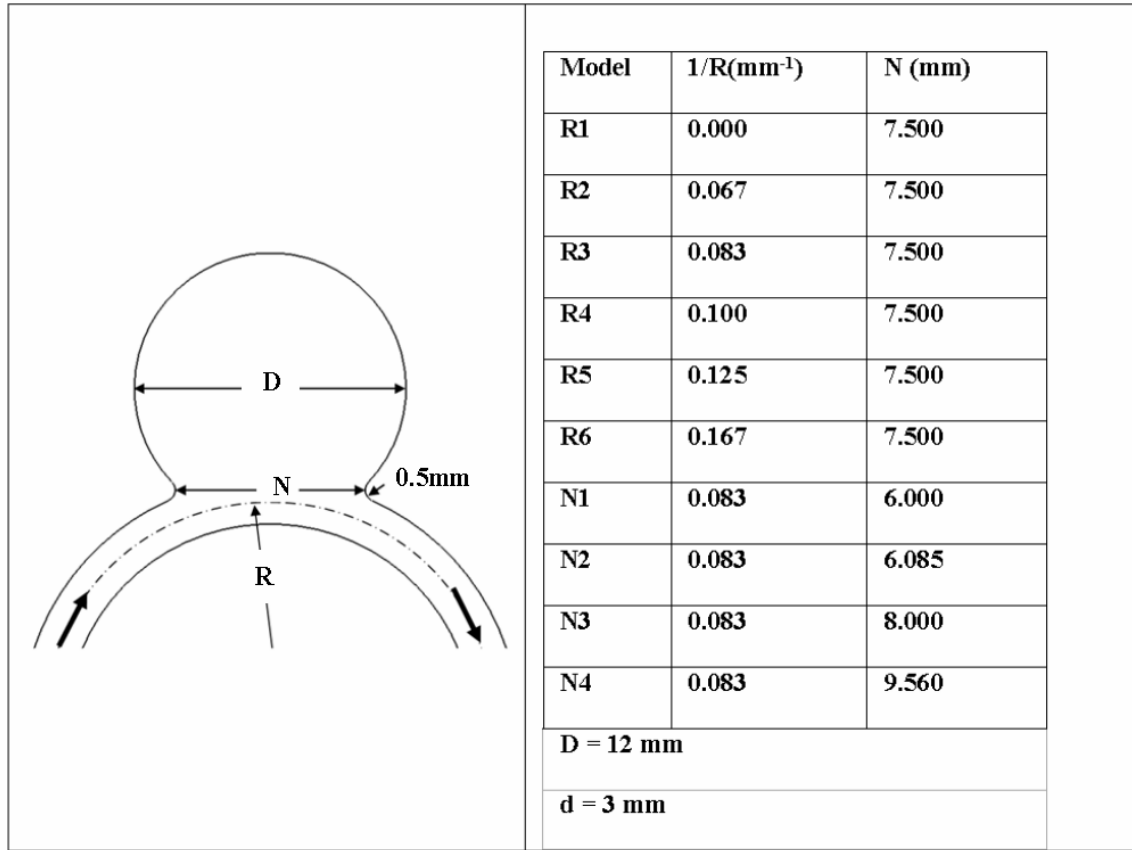


Figure 3.1: Geometrical representation of aneurysm on a curved artery. $1/R$ is the curvature of parent artery, D is the diameter of the aneurysm, N is the major axis of the aneurysm orifice and d is the internal diameter of the parent artery. The letters R1-R6, N1-N4 represent different aneurysm models. The flow direction is indicated by the arrows.

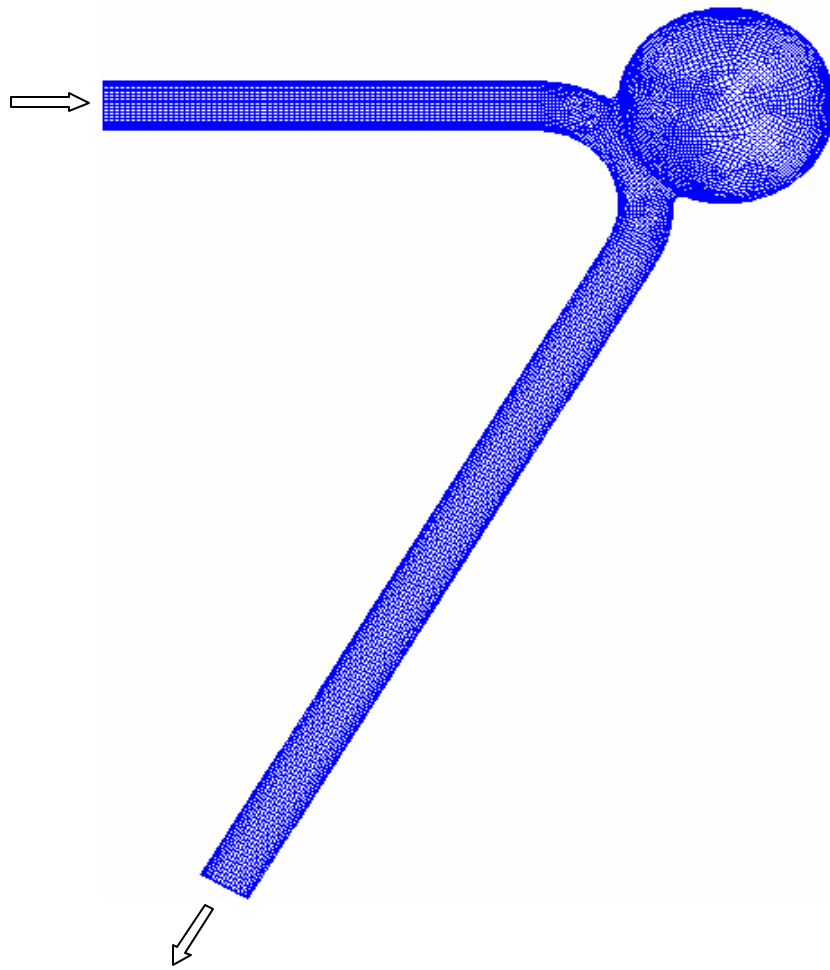


Figure 3.2: Computational mesh of aneurysm on curved artery.

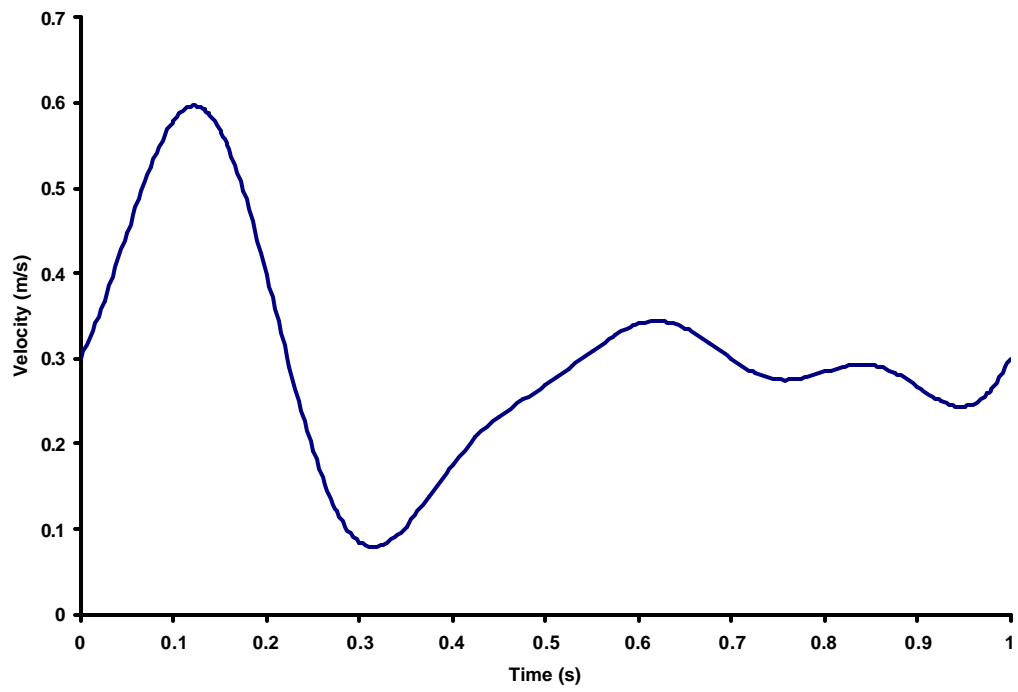


Figure 3.3: The assumed waveform that matches a physiological cerebral waveform used in the pulsatile flow simulation.

Chapter 4 Results

In this study, both steady-state and pulsatile flow simulations were conducted. The solutions were calculated using either single processor or 4 processors from SGI Origin 3800 in Center for Computational Research (CCR), University at Buffalo. The characteristics aneurysmal flow parameters were quantified.

Aneurysm flow is a highly complex 3D phenomenon. The flow dynamics can be visualized by tracking the paths of blood particles. A group of uniformly distributed blood particles were released from the inlet boundary of the computational domain (Figure 4.1). Some of the blood particles never entered the aneurysm. All of those that entered the aneurysm did so near the distal neck. Of the blood particles which entered the aneurysm, some left at the proximal neck with a lower velocity; whereas others joined the inflow from the feeding artery entered the cavity again, and whirled irregularly within the aneurysm. These highly complex blood particle paths indicate that aneurysm flow is a highly complex 3D phenomenon.

Flow impingement intensifies with increasing curvature. Figure 4.2 shows snapshots of flow velocity vectors on the center plan of symmetry captured at peak systole in models with different curvatures. The simulations showed that the velocity at the inflow zone was relatively close to the maximum velocity in the parent artery. When the curvature is insignificant or even zero (as in the case of straight vessel model R1), the flow into the aneurysm is driven primarily by viscous diffusion. In arteries with more pronounced curvature, the velocity profiles are naturally skewed toward the outer wall, indicating the effect of centrifugal force in all models. Flow enters the aneurysm from the distal neck, primarily driven by the inertia of the blood. As the artery becomes more tortuous or

aneurysm neck size increases, a larger volume of higher momentum blood impinges more strongly on the distal neck of the aneurysm. The high momentum blood forms a strong vortex in the aneurysm cavity. The distal neck can be thought of as a flow divider.

Impact zone size increases with curvature, aneurysm neck size and flow rate.

Figure 4.3 shows that the flow impingement elevates the WSS at the distal neck as a result of increasing either curvature or aneurysm neck size. It is clear that the aneurysm dome does not have uniform WSS distribution. The *area* on the aneurysm wall that experiences elevated WSS increases in size with stronger flow impingement. This size of impact zone appears to be a function of arterial curvature and aneurysm neck size. To quantify this relationship, the size of the impact zone as a function of arterial curvature and aneurysm neck size was plotted (Figure 4.4).

Figure 4.4 shows the relationship between the size of impact zone at peak systole and geometrical variable N^3/R . As shown from this figure, the impact zone increases linearly with the parent artery curvature ($1/R$). It also increases with the third order of aneurysm neck size (N). Figure 4.5 shows the relationship of impact zone and parent artery curvature at different Re . Evidently, higher flow rate may result in more intensified flow impingement on the aneurysm wall, thus, generate a larger impact zone.

Impact zone changes during a cardiac cycle. Figure 4.6 shows the change of impact zone shape during a cardiac cycle. This impact zone changed dynamically during the cycle and enlarged with the arterial curvature. The more tortuous the vessel, the larger the size of impact zone.

Time-averaged pulsatile flow solution is equivalent to steady-state flow simulation. The time-averaged pulsatile velocity profile distribution was computed and compared with steady-state flow velocity profile. There was no substantial difference

between the profiles (Figure 4.7). In addition, the steady-state simulation with Re corresponding to the maximum systole in the pulsatile flow simulation yielded the same results. The velocity profile and WSS distribution were compared in Figure 4.8.

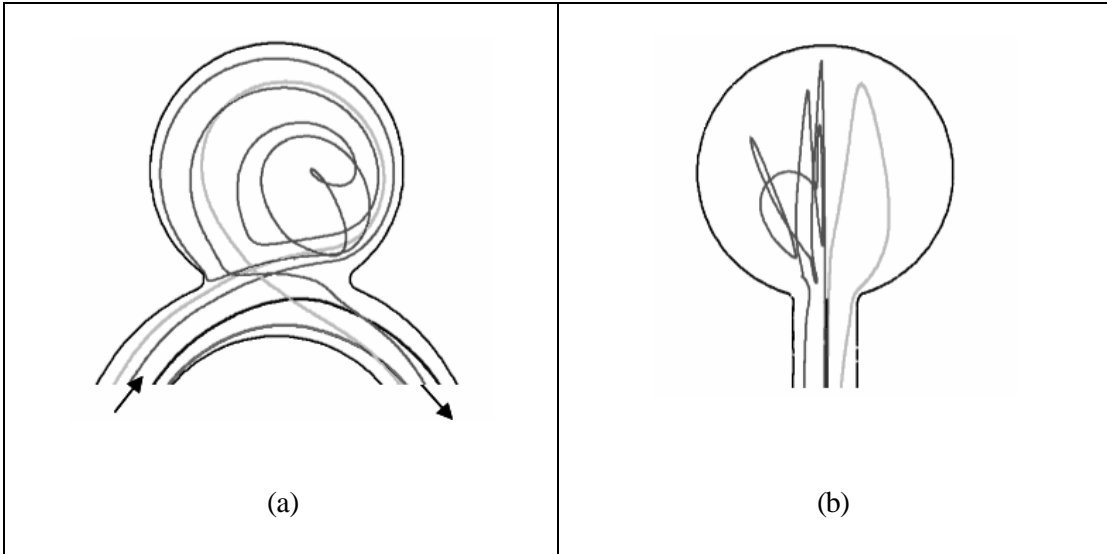


Figure 4.1: Blood elements paths in model R5 at steady state. Some blood elements never enter the aneurysm whereas others enter the aneurysm from distal end. Of those which entered the aneurysm, some leave at the distal neck, whereas others join the inflow and whirl irregularly inside the aneurysm. The blood elements flow (a) from left to right and (b) out of paper.

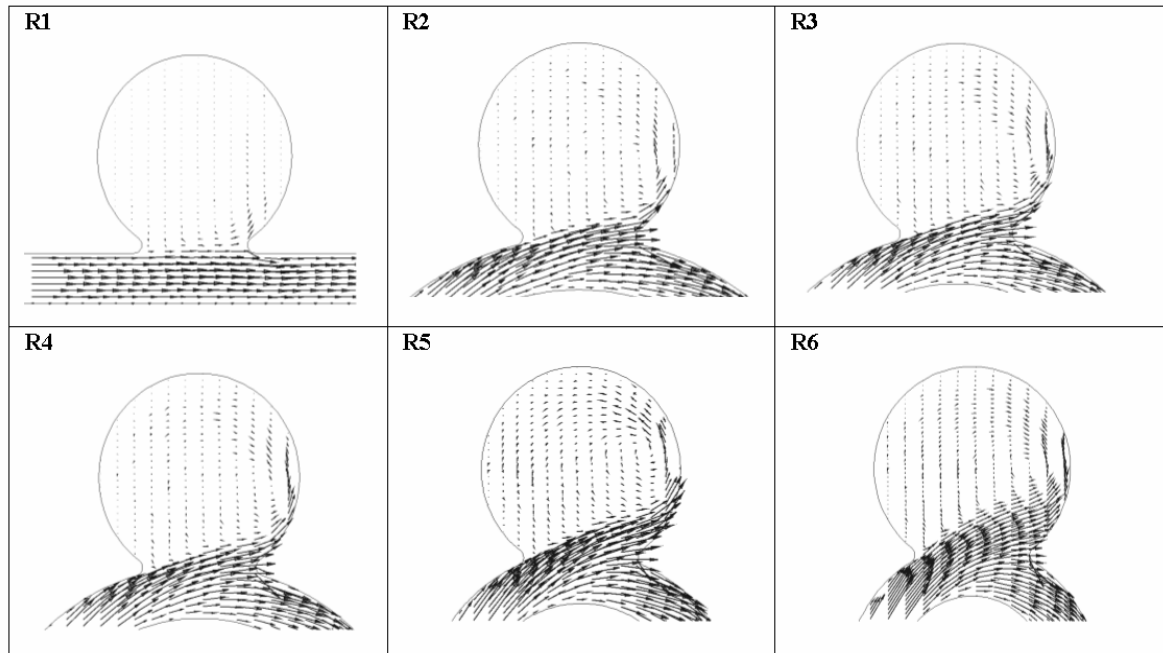


Figure 4.2: Comparison of velocity field in the symmetry plane of different models at peak systole. As the arterial degree of curvature increases, flow impingement on the distal neck intensifies. The flow flows from left to right.

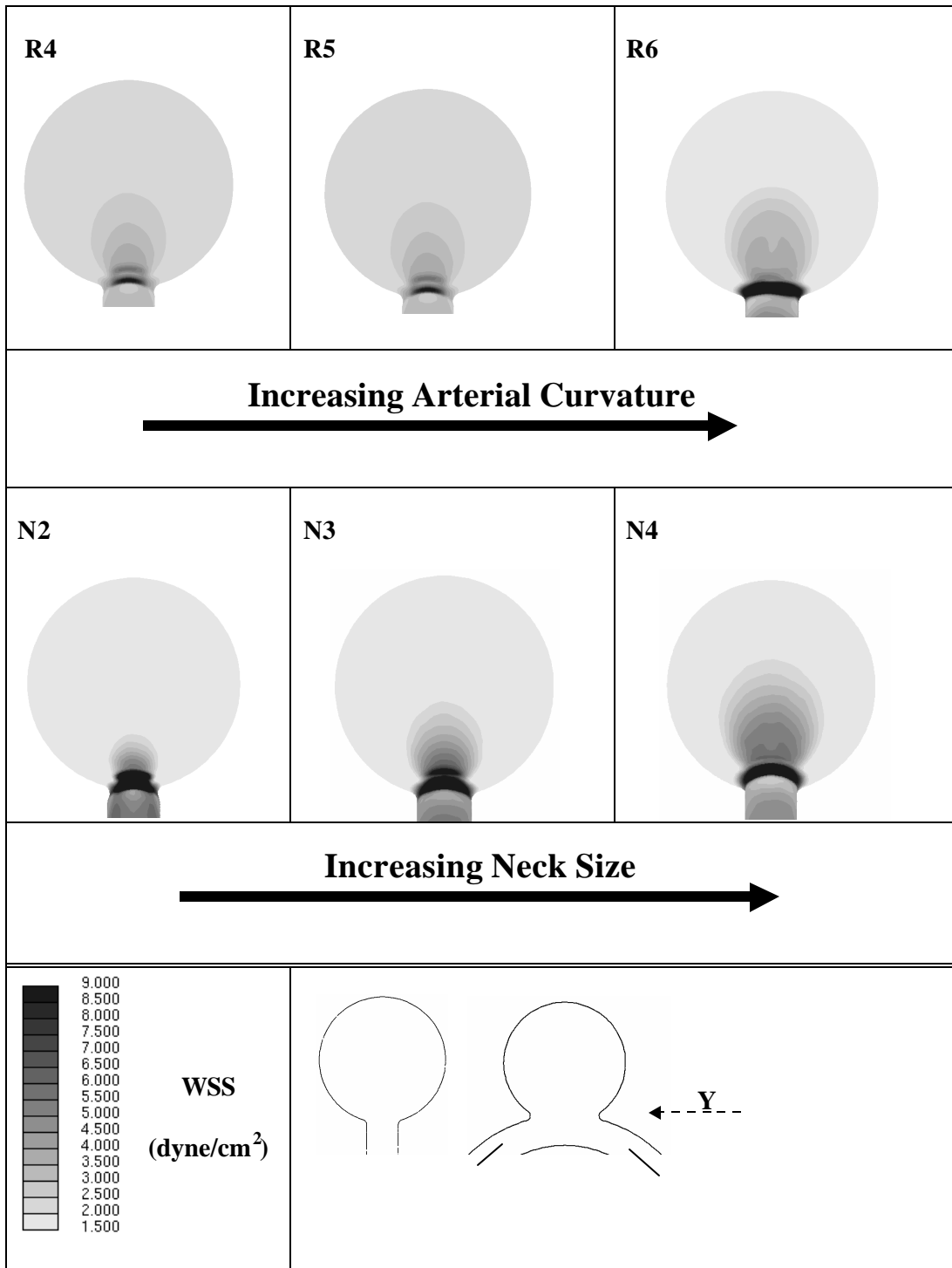


Figure 4.3: WSS distribution at the distal neck of model R5, R4, R1, N2, N3, and N4 at maximum systole of pulsatile flow simulations. The figures shown here are viewed from the Y direction, looking at the distal dome and neck.

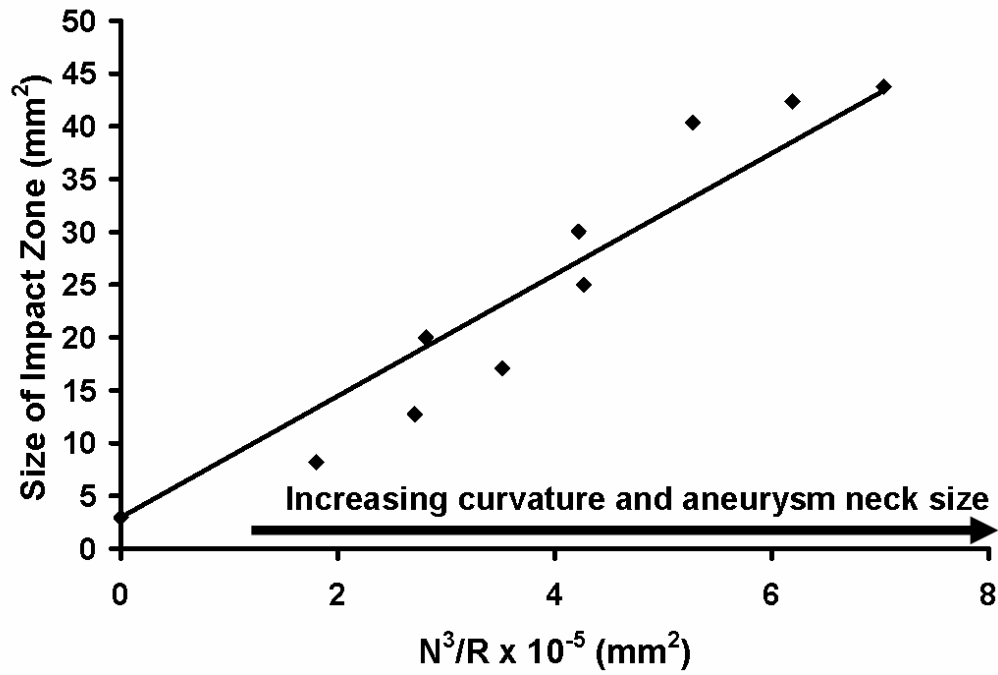


Figure 4.4: The size of impact zone at peak systole as a function of aneurysm neck size (N) and curvature (1/R). A larger aneurysm neck size on a more tortuous artery may promote artery remodeling and an increased likelihood of aneurysm growth.

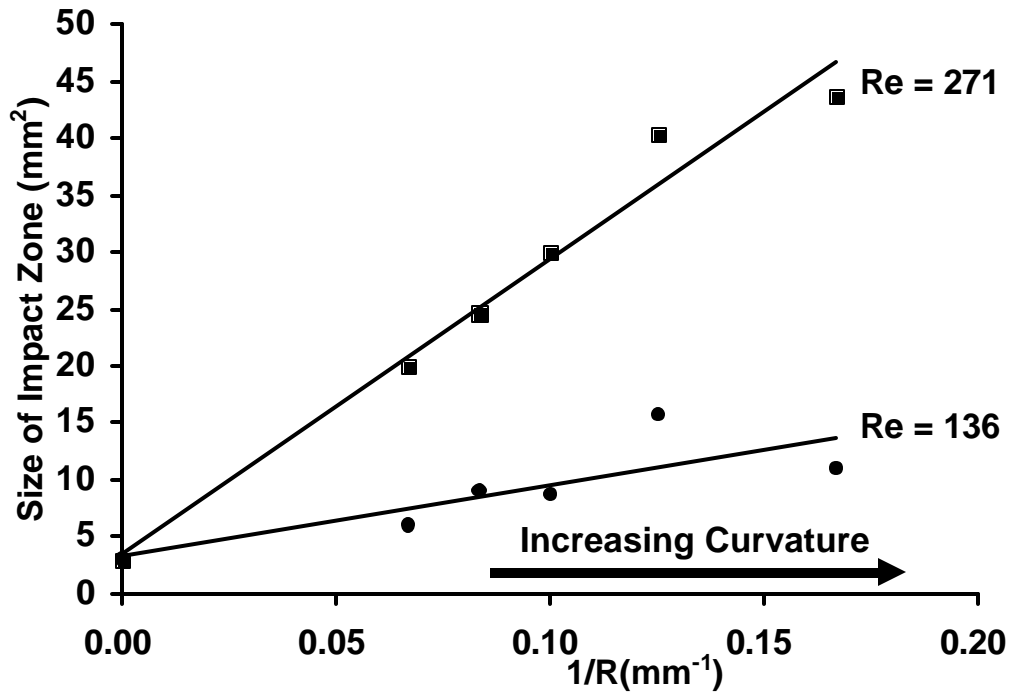


Figure 4.5: With increasing curvature (greater tortuosity), the size of impact zone increases approximately linearly. Higher degrees of arterial curvature or higher flow rate may induce more active arterial remodeling and promote aneurysm growth.

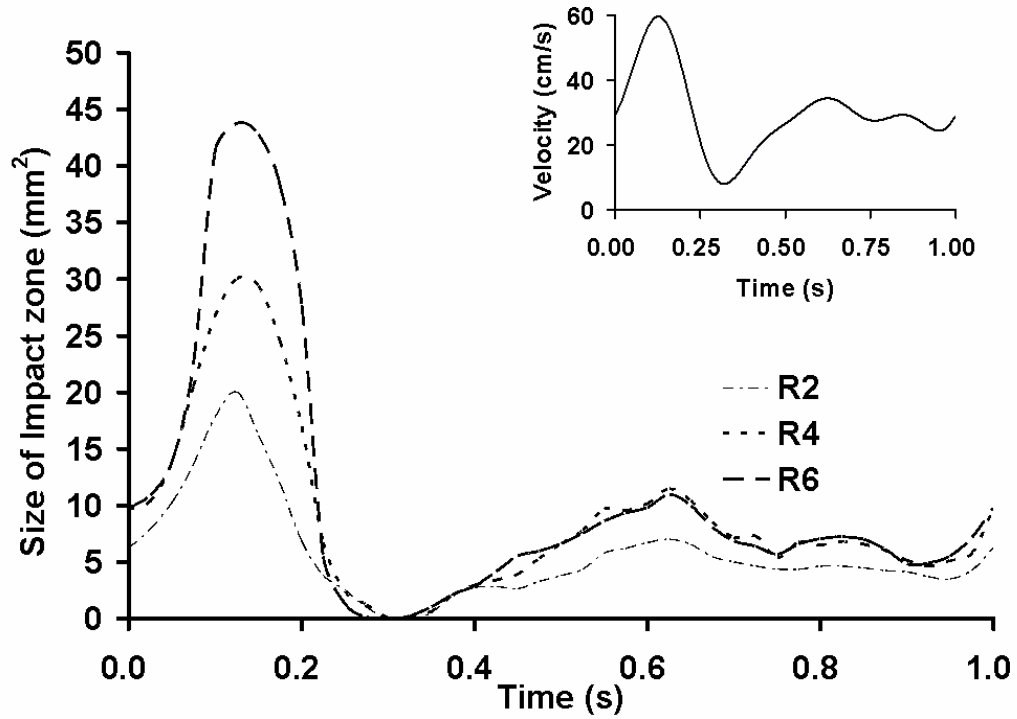


Figure 4.6: The size of impact zone at the distal neck, in which the WSS was greater than 20 dyne/cm², changed dynamically during a cardiac cycle. This variation is more pronounced with increasing arterial curvature from model R2 to R6.

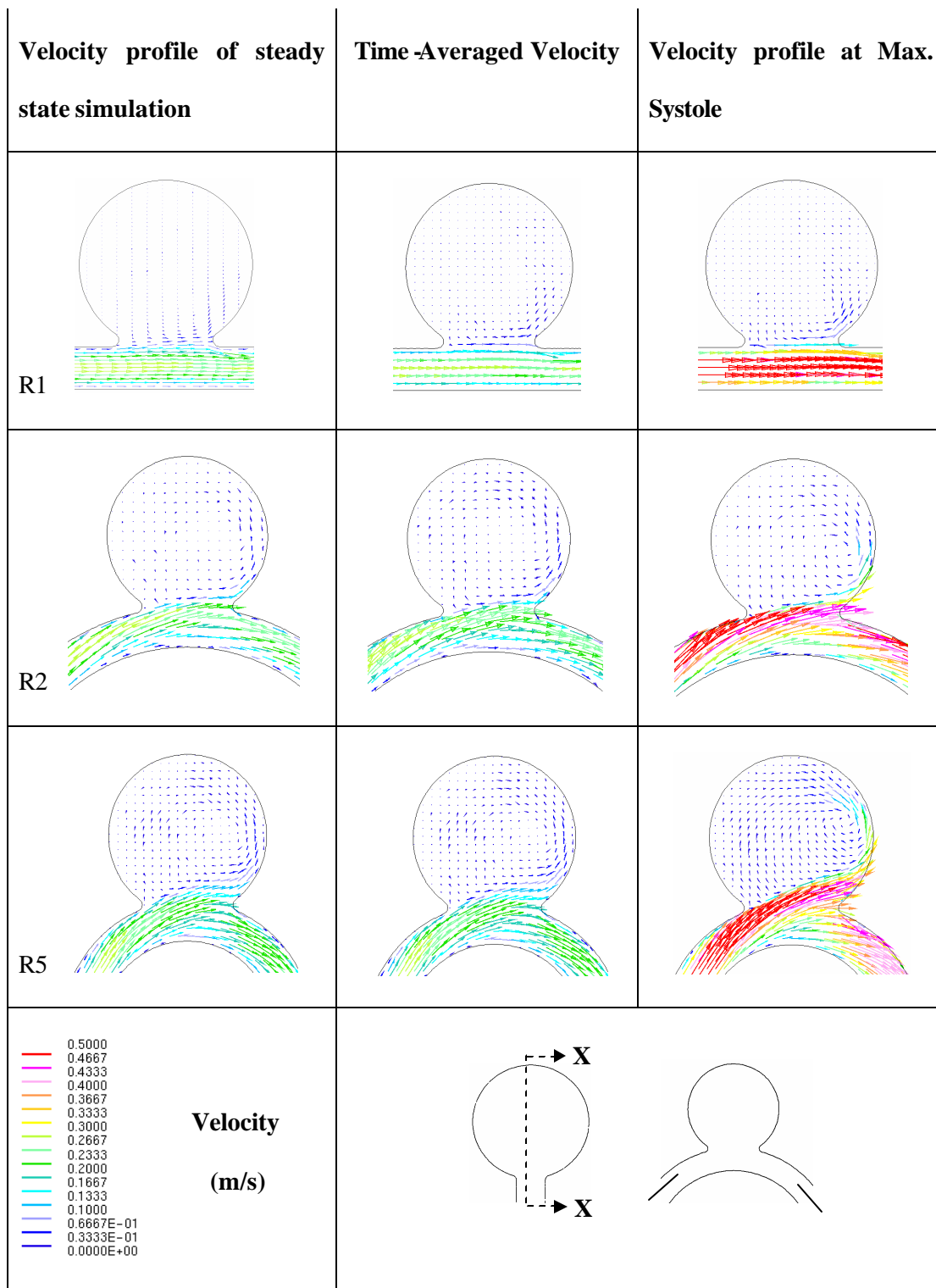


Figure 4.7: Velocity vector field in model R1, R2, and R5 at steady state, time -averaged and maximum systole of pulsatile flow simulations. The figures displayed the plane X-X (symmetry plane) of aneurysm. The flow flows from left to right.

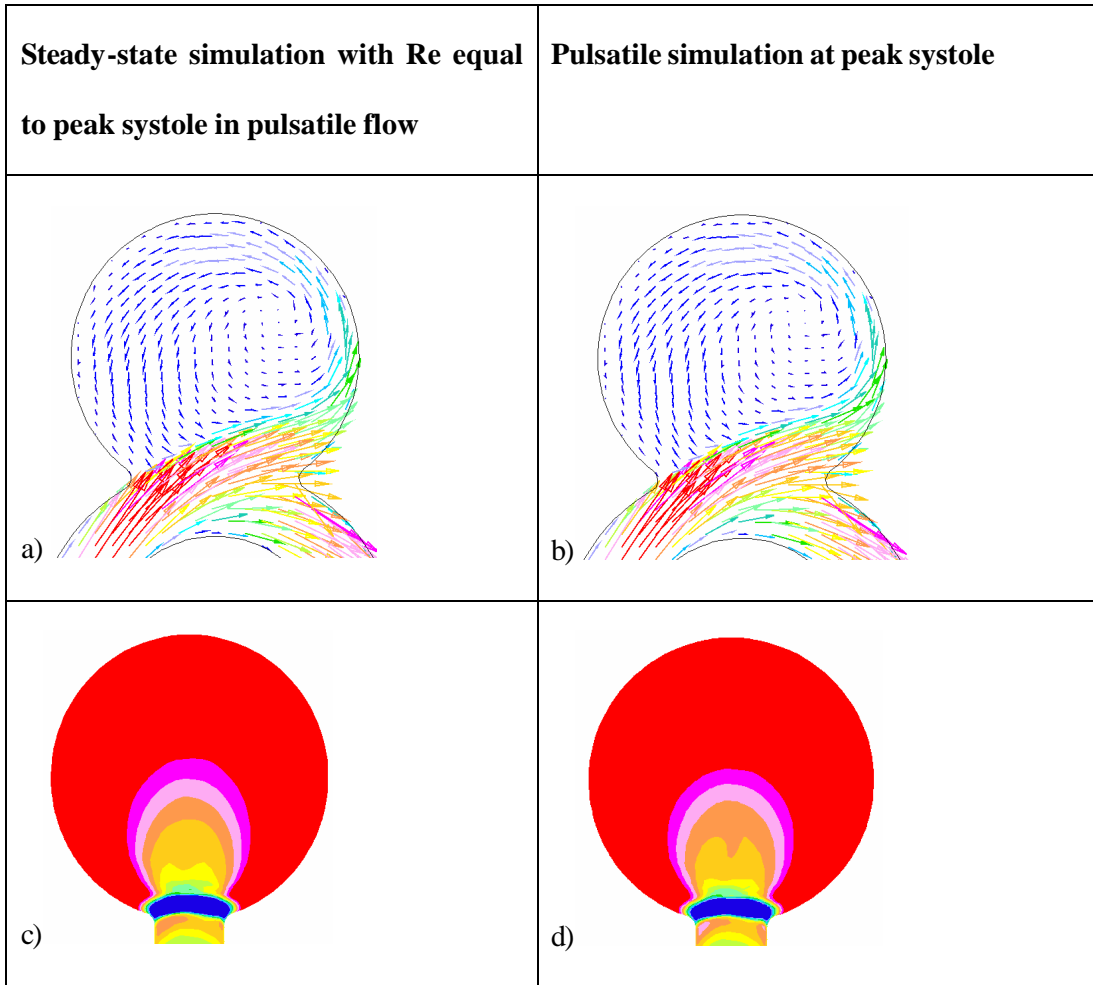


Figure 4.8: Comparison of velocity profile and WSS distribution of model R6 a,c) steady state simulation with Re equal to maximum systole in pulsatile flow, and b,d) pulsatile simulation at peak systole. The flow flows from left to right.

Chapter 5 Discussions

The progression of aneurysm is closely related to local hemodynamic environment. The hemodynamic forces resulting from flow impingement at the curved artery could be an important factor in the focal degeneration of internal elastic membrane of artery leading to aneurysm formation [22, 29, 40, 46, 48]. These hemodynamic forces are highly influenced by the flow pattern and the aneurysm geometry. Therefore, the aim of this study is to investigate the effects of arterial geometry and hemodynamic parameters in intracranial aneurysm using CFD.

5.1. Influence of Elevated WSS on Aneurysm Dilation

The continuous inclusion of a previously healthy vessel wall near the aneurysm distal neck is critical to growth and dilation of the aneurysm. The simulations have shown that flow impingement elevates both pressure and WSS at the distal neck of a sidewall aneurysm. The endothelial cells at the flow impingement zone respond to the elevated WSS by releasing vasodilation factors to remodel the wall in an attempt to return the WSS to baseline levels of 15 to 20 dynes/cm.² [60-66] These factors, including nitric oxide (NO), prostacyclin (PGI₂), and matrix metalloproteinases (MMP), degrade the extracellular matrix and dilate the arterial wall by relaxing the smooth muscle cells at the flow impingement zone.[22, 69-73, 79] The absence or disorganization of key extracellular matrix components, mainly collagen and elastin, decreases the mechanical strength of the aneurysm wall. In addition, the elevated pulsatile pressure plays a role in stretching and expanding the aneurysm wall. [9] The weakened aneurysm wall, in conjunction with the stretching from this pressure, becomes more susceptible to dilate.[29, 30, 74] Furthermore, as the aneurysm wall continues to degrade and be stretched from the distal neck, more

healthy vessel from the parent artery will be incorporated in the aneurysm. As a result, the aneurysm will grow larger, continuously experience flow impingement, and undergo the degradation and stretching process. This finding is in agreement with the concept that intense flow impingement induces degeneration of arterial wall components, leading to aneurysm dilation. [22, 29, 40, 46, 48]

The arterial curvature appears to be responsible for the major development of the impact shear zone. The varying level of shear stress at the aneurysm wall at different sites may indicate varying likelihood of aneurysm formation, growth, and rupture [47]. The consequences of continuous blood flow impingement and large impact shear zone are aneurysmal growth and regrowth of a treated aneurysm.

5.2. Risk of Aneurysm Growth Increases with Increasing Arterial Curvature

Aneurysms located at a position on the vessel with a high degree of arterial curvature may have a higher risk of accelerated growth. The simulations have shown that as the degree of parent vessel curvature increases, flow impingement intensifies, leading to an increase in the *area* of the elevated WSS. It is reasonable to expect that with an increasing *area* of elevated WSS, the quantity of vascular remodeling factors released also increases accordingly. In an attempt to restore the elevated WSS to the baseline level, the increase in the quantity of vascular remodeling factors leads to a more rapid remodeling process, as mentioned earlier. Ultimately, these remodeling factors will result in a higher likelihood of wall injury and aneurysm growth. [24-30, 76, 89] Therefore, aneurysms located at a position on the vessel with a high degree of curvature are suspected to be susceptible to a greater risk

of continuous growth. These 3D simulations should provide a more accurate quantification of the hemodynamics than aneurysm studies based on 2-dimensional CFD models.

5.3. Therapies Developed for Aneurysms on Straight Vessels May Not be Effective for those on Curved Vessels

The introduction of vascular stents to aid in coiling has opened the door to aneurysm thrombotic occlusion via stenting. Geremia *et al.* and Wakhloo *et al.* demonstrated complete occlusion of sidewall and fusiform aneurysms on carotid arteries in canines by using stents alone. [80-82] However, these experiments were based on aneurysm located at straight vessels. It is possible that stenting or coiling the sidewall aneurysms located at vessels with a high radius of arterial curvature will not tend to induce the stable thrombus formation observed in straight vessels as a result of significantly different flow mechanisms.

For a sidewall aneurysm located on a straight vessel, the flow entering the aneurysm is predominantly shear driven. The vorticity at the proximal aneurysm neck weakly entrains the flow into the aneurysm. On the other hand, for an aneurysm on a curved vessel, the inertia of the blood flow (centrifugal effect) drives the flow to travel along the curve. This inertia-driven mechanism produces a stronger flow impingement on the distal neck and generates a coherent vortex within the aneurysm.

Therefore, low momentum flow entering a lateral aneurysm on a straight or small degree of curvature creates a stasis-like environment and increases the tendency to thrombosis. [58] This in turn increases the likelihood of a successful treatment. A lateral aneurysm located on a vessel with a high degree of arterial curvature continues to refresh the blood and decrease the blood residence time in the aneurysm cavity. [77] As a result, according to the simulations, aneurysms on vessels with a high radius of curvature may not

tend to induce stable thrombus formation and this type of aneurysm has a greater risk of growth and should be treated early. Furthermore, bridging the aneurysm neck with a stent-alone may not alter the flow in an aneurysm located on a curved artery sufficiently to induce thrombotic occlusion due to different flow mechanisms. However, placing a stent across the aneurysm neck may straighten the vessel to some degree and thereby reducing wall shear stress at the distal neck, possibly slowing down the aneurysm growth.

5.4. Effectiveness of Endovascular Treatment and Aneurysm Geometry

In support to the flow impingement and continuous aneurysm growth, higher degrees of arterial curvature may decrease the chances of complete aneurysm occlusion in endovascular treatment. Endovascular coil embolization, has been accepted as a therapeutic alternative to surgical clipping for the occlusion of cerebral aneurysms from the circulation. [92, 93] However, loose coil packing, together with the exposure of the aneurysm neck to flow impingement, has been known to lead to incomplete occlusion in the majority of wide-necked aneurysms. [94, 96] With an increasing degree of arterial curvature, the high momentum inflow may compact the coils upon repeated impact. The pulsatile flow can push the coils and the localized adherent thrombi toward the aneurysm dome, uncovering the distal neck, where growth occurs. [83, 84, 94, 97] The incessant pulsatile flow impingement on the distal neck will result in arterial wall degradation. The stretching process mentioned previously results in the incorporation of an increasing amount of normal parent vessel into the aneurysm. Continuous flow impingement on aneurysm located at a position on the vessel with a high degree of arterial curvature will have a higher likelihood of recurrence or continuous growth. Thus, to increase the long-term patency of any endovascular treatment, interventions should be aimed at protecting the aneurysm wall from flow impingement,

sufficiently dampening the inflow momentum, and inducing a pro-thrombogenic environment.

Recent literature has indicated that aneurysms with diameters less than 10 mm should be observed, rather than treated. [98] This work indicates that aneurysms on vessels with a high radius of curvature may grow at a faster rate than their counterparts in straight vessels. The data reported in this paper suggests that asymptomatic aneurysms on high radius of curvature vessels should be monitored at regular intervals during growth and may require intervention at an earlier stage than their counterpart on straight vessels.

Chapter 6 Reconstruction of Patient-Specific Geometry

The parametric study involving minor alterations in local anatomical geometric parameters suggests that a strong correlation between the local anatomic geometry and aneurysm pathophysiology. There are no two identical aneurysms in clinical cases. Thus, the understanding of aneurysm patho-physiology is incomplete without considering the local hemodynamic environment and local anatomic geometry. [99-102] Non-invasive, *in vivo* quantification of hemodynamic parameters is very difficult and sometimes not feasible. Recently, the integration of CFD and medical images has opened new insights in studying the vascular hemodynamics.

The computer simulations can provide more insight in understanding the progression of vascular diseases, designing new endovascular interventions, and improving the durability of vascular prostheses. Using computer simulations, clinicians are able to plan, design, evaluate and advance the possible treatments to reduce the mortality and morbidity in clinical cases.

This study aims to develop the rapid, semi-automated technique to reconstruct the anatomically realistic aneurysm geometry from patient's diagnostic images for CFD analysis. This is a stepping stone to generate a framework to facilitate clinicians selecting the treatment options scientifically (Figure 6.1). The patient's diagnostic images will be used to reconstruct the 3D realistic vessel geometry. Both CFD and experimental analysis will be conducted to quantify accurately the 3D hemodynamic parameters of individual patient's geometry. The ultimate goal of motivation is to assess the patient's risk and recommend the

treatment paradigm based on the understanding of 3D aneurysmal hemodynamics. This framework will eventually advance the quality and effectiveness of therapy of individual patient.

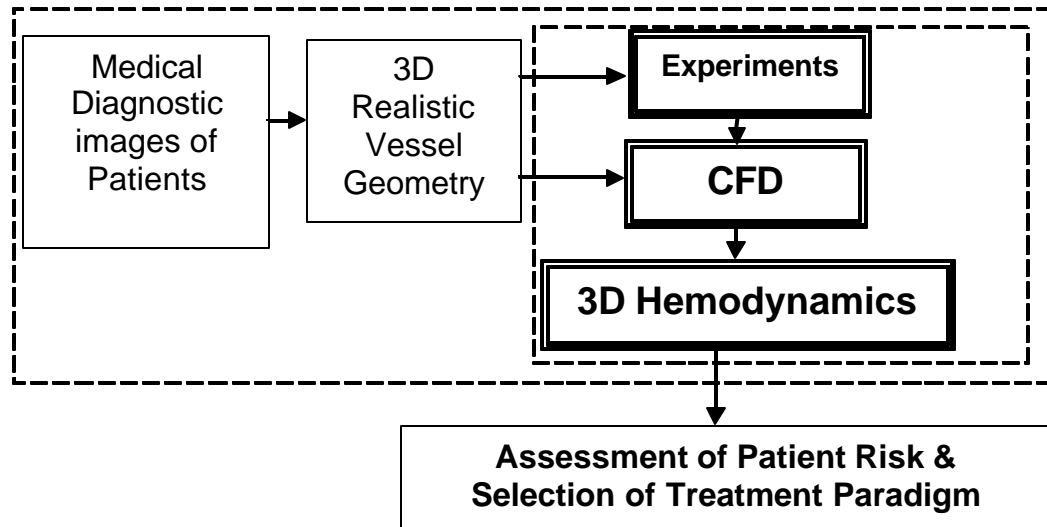


Figure 6.1: A patient-specific procedure framework to facilitate physicians to make scientifically sound clinical decisions.

6.1. Image reconstruction techniques

Vascular imaging techniques, such as computed tomography (CT), magnetic resonance imaging/angiography (MRI/MRA), X-ray rotational/conventional digital subtraction angiography (DSA) have been routinely used in diagnostic, visualization and surgical planning. However, the integration of 2D medical images and CFD analysis is not trivial

There are a variety of methods to segment the 2D medical images and reconstruct the 3D geometry for CFD analysis. The most commonly used method to reconstruct the 3D geometry is edge detection. The images of the patients are usually obtained in a series of

equal distanced 2D slices of $n \times n$ pixels. User will draw and interpolate the 2D region of boundaries from each slice, then stack these boundaries together to construct the 3D contours. These 3D contours will be smoothed and interpolated to obtain the 3D surface of the region of interest. [100, 111] The process requires a lot of operator interactions, tedious, high CPU consumption and less flexible if the original 2D image intensity is not uniform between slices. [111] In addition, the patients must be stationary during the image acquisition. Errors due to patient random movement are difficult to be corrected.

6.2. 3D Image Reconstruction from Biplane Angiography

To reduce time, costs and operator interactions, a new technique was devised to reconstruct the patient's 3D aneurysm geometry from biplane angiography images. In this study, a patient presented with double vision which eventually led to a cerebral angiogram showed a large left posterior inferior cerebellar artery. (Figure 6.2)

The biplane angiography images (512 pixel x 512 pixel) of the aneurysm were acquired using Toshiba biplane DSA unit. In each image, approximately 510 points were indicated manually along the vessel centerline. After the points along the vessel were indicated, the vessel centerline points between each pair of indicated points are determined automatically using a modified sector method. [113, 115, 116] Using these points, imaging geometry was calculated by Procrustes algorithm. [117] Finally, an epipolar line technique was used to determine the corresponding points along the vessel centerlines in the biplane image pair. [113, 114] Vessel radii were calculated at each centreline point using edge detection on vessel profiles extracted perpendicular to the 2D centrelines. With the 3D centerline as centers, these radii were used to approximate the vessel lumen. The 3D positions of vessel lumen and aneurysm boundaries were exported individually for model reconstruction.

The lumen of both vessels and aneurysm geometry were imported as datum curves in Pro-Engineer® for surface reconstruction. A user-defined program was created to convert the 3D positions into datum curves. (Appendix) In Pro-Engineer®, these datum curves were individually selected to generate the circumferential surface of the vessel and aneurysm. Finally, both vessel surface and aneurysm surface were merged and exported in IGES format.

6.3. Computational mesh

The anatomically realistic aneurysm geometry in IGES format was imported into Gambit® for mesh generation. Since the imported model in Gambit® contained only surfaces, a solid volume was constructed using these surfaces in Gambit® before mesh generation. The cross-sectional surface of the vessel and the aneurysm were created in Gambit®. Then closed volumes were defined using the surfaces. Once the solid volume was generated, the boundary layers of the model were first constructed. Then the surfaces and the volume were meshed using tetrahedral mesh (Figure 6.3). Finally, the computational mesh was exported and used for CFD simulation in STARCD®.

6.4. Computational Methodology

In the CFD simulation, incompressible, laminar and Newtonian flow properties were assumed in the rigid aneurysm model. The assumed flow density and viscosity were 1060 kg/m^3 and 0.0035 kg/ms , respectively. Since the corresponding anatomically realistic cardiac waveform of the artery was not recorded during image acquisition, steady-state simulation was conducted in this study. Velocity of 0.4 m/s was assumed at the inlet of the computational domain whereas zero pressure gradients were assumed at the outlet of the computational domain. Implicit scheme was chosen for the simulation. Hemodynamic

parameters (including velocity, blood particle paths, and pressure) were determined from the simulation results.

6.5. CFD Analysis

Visualizing the 3D hemodynamic parameters of giant, complex aneurysm geometry is not trivial. The flow field was represented by a group of 3D blood particles paths traveled in the aneurysm (Figure 6.4). These massless and non-diffusing particles were released at equal distance of 0.2mm from the centerline of the inlet. The preliminary simulation showed that the flow inside this giant aneurysm was relatively undisturbed compared with the flow in the artery. Consistent with the previous studies of aneurysmal flow, the blood particles entered the aneurysm from the distal neck. However, due to large aneurysm size, the flow velocity reduced significantly inside the aneurysm, which produced a stasis-like flow environment. The blood particles swirled irregularly inside the aneurysm before leaving the aneurysm. This, obviously, increased the particle residence time in the aneurysm.

6.6. Discussions

In an attempt to explore the hemodynamic of patient-specific aneurysm, the preliminary simulation showed that the flow is significant dependent on the geometry of the aneurysm. Clinical cases have discovered that some giant, ruptured aneurysms have thrombus formed inside the aneurysm sac. However, it is unclear why the thrombus was formed and whether the thrombus played a role to protect the aneurysm through self-occlusion. The preliminary simulation showed that the large aneurysm volume produced a stasis-like environment and increased the blood residence time. This type of hemodynamic environment is favorable to thrombus formation. Therefore, thrombus formation is not

unusual in giant aneurysms. However, due to mixing and increased flow activity in the aneurysm, the mechanism of thrombus formation may be disturbed. Consequently, the geometry of giant aneurysm may favor the thrombus formation in some regions, the thrombus formed is not sufficient to achieve self-occlusion in this study.

Large volume of flow occupied the aneurysm may induce additional loads to the surrounding tissues, thereby causes headache or double-vision to the patient. Furthermore, the large volume of flow also increased the intra-aneurysmal pressure, which thereby increased the stresses in the aneurysm wall. Accordingly, when the stresses in the aneurysm wall exceed its strength, rupture occurs. Therefore, clinicians always treat a giant aneurysm with greater urgency, since it carries a higher potential of rupture and the thrombus, when breaking into emboli, may lead to strokes.

6.7. Limitations

The aneurysm and vessel lumen are reconstructed individually. When both lumens are put together, the common interface, which is aneurysm neck, is not well-defined. High resolution images taken from rotational angiography could be used to improve the geometry of both the vessel and aneurysm lumen. In addition, since large aneurysms could have formed thrombus, the aneurysm geometry obtained from DSA images, may not represent the exact aneurysm geometry.

Although the preliminary simulation provided new insights of interactions between hemodynamic forces and vascular geometry, the accuracy of the reconstructed 3D model has not been addressed. If the resolution is low, the surfaces of the reconstructed solid model become very rough and irregular. Such situations could lead to artifacts, and difficulty in

mesh generation. However, by smoothing the surfaces or by generating surface using NURBS, the difficulty of mesh generation could be improved.

To virtually reconstruct the anatomically realistic hemodynamic environment, the pressure or velocity waveform must be extracted from the region of interest. With pulsatile flow in arterial curvature and bifurcation sites, the hemodynamic stresses are strongly dependent on the blood flow velocity.

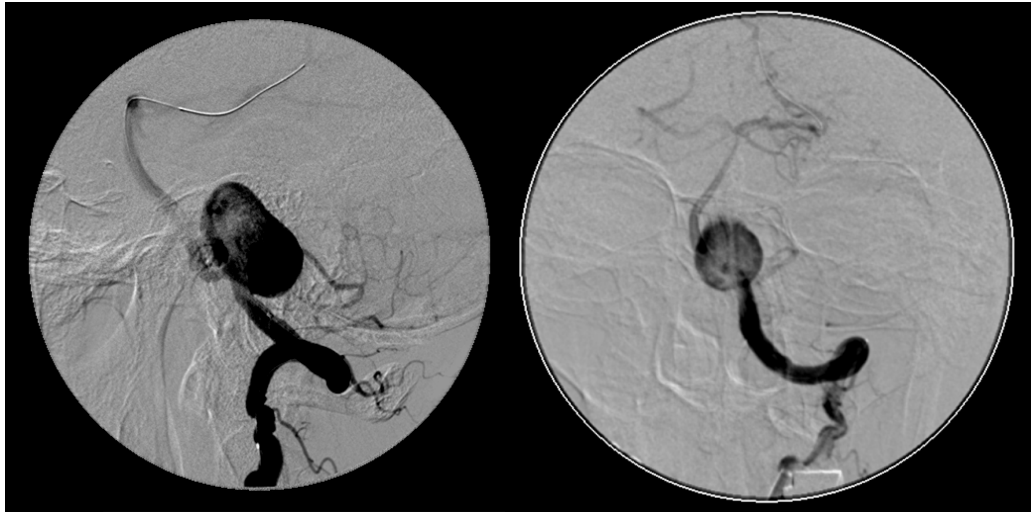


Figure 6.2: A patient-specific aneurysm model from angiography

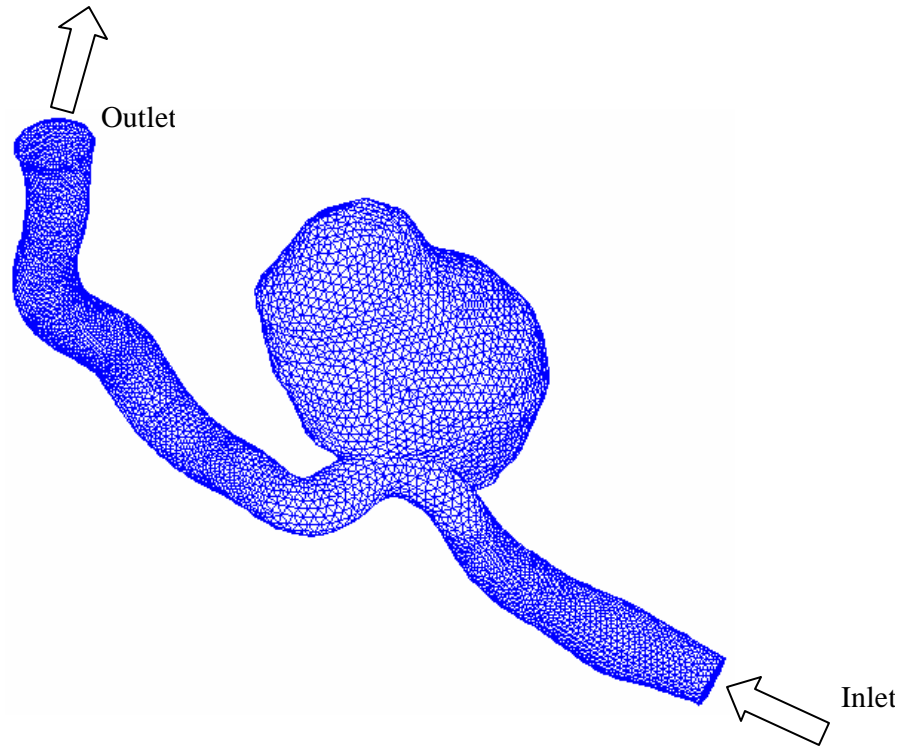


Figure 6.3: The computational mesh of patient-specific aneurysm geometry.

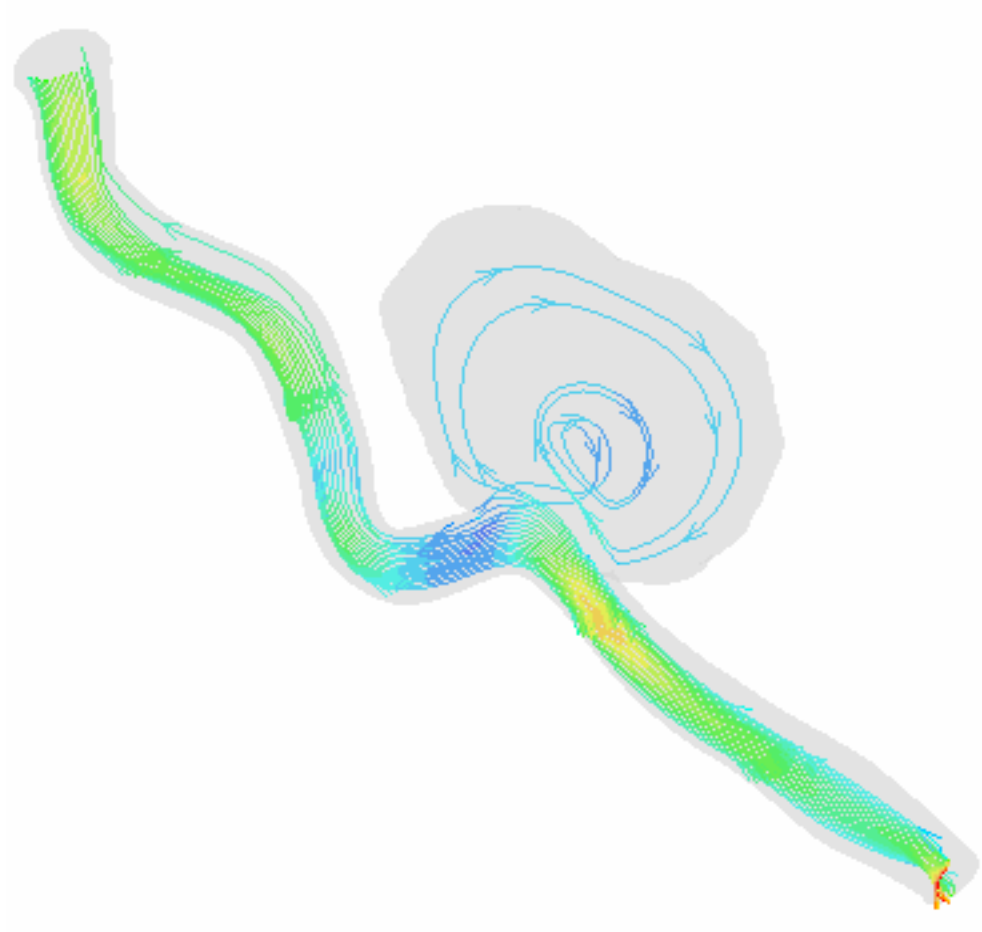


Figure 6.4: The CFD simulation of blood particle paths in patient-specific aneurysm.

Chapter 7 Conclusions

The CFD study revealed that the aneurysm located on a high degree of arterial curvature experienced more intensified flow impingement on the aneurysm wall. Wide-neck aneurysms on a curved artery experienced the most intensified flow impingement and thereby potentially have an increased likelihood of aneurysm growth. This analysis has shown that hemodynamic stresses are time-dependent and can vary greatly over the course of the cardiac cycle and at different locations of an aneurysm. Furthermore, this parametric study involving minor alterations in local anatomical geometric parameters suggests that a strong correlation between the local anatomic geometry and aneurysm patho-physiology. In addition, the local hemodynamics of an aneurysm is believed to affect the progression of aneurysm growth and effectiveness of endovascular treatments. A large impact zone on the aneurysm wall is potentially implicated as the most likely site of aneurysm initiation and growth or regrowth of a treated aneurysm. To occlude an aneurysm successfully and prevent regrowth, it is critical to protect the impact zone and impede the inflow from the artery. The integration of CFD simulations with medical diagnostic imaging techniques assesses new insights to the pathogenesis of aneurysm on an individual basis. [99-102] This forms the basis to advance the knowledge of aneurysm hemodynamics, predicts the outcome for surgical procedures, and assesses patient-specific risks.

Chapter 8 Future Considerations

Although the current CFD solver gave reasonable good results, the solutions should be validated using experimental results. Particle image velocimetry (PIV) or Laser Doppler velocimetry (LDV) can be conducted to validate the CFD results. The flow velocity should be validated first. Then the WSS value should be experimentally calculated from the velocity gradients. The detailed 3D WSS contour map should be obtained from 3D velocity measurements using Stereoscopic PIV (SPIV) or Holographic PIV (HPIV).

In order to obtain more accurate results, it is recommended that the mesh of the computational domain is refined at location with large velocity gradients. Mesh refinement should be automated to reduce time, costs, and user interventions. In addition, due to numerical truncation and round-up, these errors should be quantified.

Furthermore, to verify the postulations and to better understand the biological response of aneurysm wall in different hemodynamic environment, a series of *in vivo* experiments should be conducted. A detailed protocol in creating aneurysms in the *in vivo* experiments will first be developed. The animal aneurysm models should mimic the gross appearance of human cerebral aneurysms. The growth of the aneurysms should be monitored at regular intervals using conventional or rotational digital subtraction angiography. The anatomically realistic aneurysm geometry, created from *in vivo* experiments, should be extracted for detailed CFD and *in vitro* analysis.

Computational modeling will enable clinicians to make treatment decisions that are quantitatively based, drastically cutting down risk of failure or need for re-treatment and design interventions on individual basis. The realistic aneurysm geometry databank should be first set up. The virtual 3D aneurysm geometry in the databank should be easily access

for detailed CFD analysis. In addition, the patients' follow-up should be performed at regular interval to correlate the *in vitro* modeling results and *in vivo* hemodynamic environment. This will enable us to improve the effectiveness of interventions.

Appendix

Inlet boundary condition for pulsatile flow simulation

```
C*****
      SUBROUTINE BCDEFI(SCALAR,U,V,W,TE,ED,T,DEN,TURINT)
C      Boundary conditions at inlets
C*****
C      STAR RELEASE 3.150
      INCLUDE 'comdb.inc'
      COMMON/USR001/INTFLG(100)
      DIMENSION SCALAR(50)
      LOGICAL TURINT
      INCLUDE 'usrdat.inc'
      DIMENSION SCALC(50)
      EQUIVALENCE( UDAT12(001), ICTID )
      EQUIVALENCE( UDAT04(002), DENC )
      EQUIVALENCE( UDAT04(003), EDC )
      EQUIVALENCE( UDAT02(005), PR )
      EQUIVALENCE( UDAT04(005), PRC )
      EQUIVALENCE( UDAT04(009), SCALC(01) )
      EQUIVALENCE( UDAT04(007), TC )
      EQUIVALENCE( UDAT04(008), TEC )
      EQUIVALENCE( UDAT04(059), UC )
      EQUIVALENCE( UDAT04(060), VC )
      EQUIVALENCE( UDAT04(061), WC )
      EQUIVALENCE( UDAT04(064), UCL )
      EQUIVALENCE( UDAT04(065), VCL )
      EQUIVALENCE( UDAT04(066), WCL )
      EQUIVALENCE( UDAT02(070), X )
      EQUIVALENCE( UDAT02(071), Y )
```

```
EQUIVALENCE( UDAT02(072), Z )
```

```
C-----
```

```
REAL DG, F1H, SEH, THH, FOH, RAD, VMAX
```

```
DG = 360*TIME + 2
```

```
RAD = 3.1416/180
```

```
F1H = 0.78*COS(DG*RAD-(39/60)*RAD)
```

```
SEH = 1.32*COS(2*DG*RAD-(82.75*RAD))
```

```
THH = -0.74*COS(3*DG*RAD+(26.5*RAD))
```

```
FOH = -0.41*COS(4*DG*RAD-(16.5*RAD))
```

```
VMAX = 0.1*(F1H + SEH + THH + FOH) + 0.3
```

```
U = VMAX * (1 - ((X**2+Z**2)/0.0015**2) )
```

```
RETURN
```

```
END
```

```
C
```

Program used for importing the geometry to Pro/Engineer®

```
#include <iostream.h>
#include <fstream.h>
#include <iomanip.h>
ifstream inputfile;
ofstream outputfile;

int main()
{
double c[20000][3];
int n, i, j,k,l;
double x,y,z, scale;
cout.setf(ios::fixed);
cout.setf(ios::showpoint);
n=17100;
for (i=0;i<=n;i++)
{
c[i][1]=0;
}

inputfile.open("aneurysm_cm.txt");
outputfile.open("aneurysm_cm.ibl");
outputfile << "Open\n" << "Arclength\n";
outputfile << "Begin section !\n" << "Begin curve !\n";

for (int i=0; i <n; i ++)
{
for (int j=0; j<3; j ++)
```

```

        inputfile >> c[i][j];
    }
}
inputfile.close();

k=0;

l=0;

for (i=0;i<n;i++)
{
    for (j=0;j<3;j++)
    {
        outputfile << c[i][j] <<" ";

        x=c[k][0];
        y=c[k][1];
        z=c[k][2];
    }
    l=l+1;
    outputfile << endl;
    if (l % 40 ==0)
    {
        outputfile << x<<" "<<y<<" "<<z<< endl;
        outputfile << "Begin section !\n" <<"Begin curve !\n";
        k=k+100;
    }
}

outputfile.close();

return 0;

}

```

References

1. American Heart Association: *Heart Disease and Stroke Statistics -- 2003 Update*, pp. 15, 2003
2. Ronkainen A, Hernesniemi J, Puranen M, *et al.*: Familial intracranial aneurysms. *Lancet*, 349:380-384, 1997
3. Heros C, Kistler JP: Intracranial arterial aneurysman update. *Stroke*, 14:628-631, 1983
4. Kayembe KNT, Sasaharam M, Hazama F: Cerebral Aneurysms and Variations of Circle of Willis, *Stroke*, 15:846-850, 1984
5. Davies PF: Flow-mediated endothelial mechanotransduction. *Physiol Rev*, 75:519-560, 1995
6. Melkumyants AM, Balashov SA, Khayutin VM: Endothelium dependent control of arterial diameter by blood viscosity. *Cardiovasc Res*, 23:741-747, 1989
7. Kraiss LW, Kirkman TR, Kohler TR, *et al.*: Shear stress regulates smooth muscle proliferation and neointimal thickening in porous polytetrafluoroethylene grafts. *Arterioscler Thromb*, 11:1844-1852, 1991
8. Langille BL, O'Donnell F: Reductions in arterial diameter produced by chronic decreases in blood flow are endothelium-dependent. *Science*, 231:405-407, 1986
9. Burleson AC, Turitto VT: Identification of quantifiable hemodynamic factors in the assessment of cerebral aneurysm behavior. *Thromb Haemost*, 76:118-123, 1996
10. Chandran KB: Cardiovascular Biomechanics, New York: New York University Press, pp. 120, 1992
11. Pedley TJ: The fluid mechanics of large blood vessels. Cambridge University Press, pp. 13. 1980

12. Feng YC, Perrone N, Anliker M: Biomechanics: Its foundations and objectives. Prentice-Hall, 1972
13. Fukushima T, Matsuzawa T, Homma T: Visualization and finite element analysis of pulsatile flow in models of the abdominal aortic aneurysm, *Biorheology*, 26:109-130, 1989
14. Nerem RM, Braddon LG, Seliktar D, *et al.*: Tissue Engineering and the vascular system. In: Atala, A. and Mooney, D (eds), *Synthetic biodegradable polymer scaffolds*, pp. 163-185, 1997
15. Atabek HB, Ling SC, Patel DJ: Analysis of coronary flow fields in thoractomized dogs, *Circulation Engineering*, 107: 307-315, 1975
16. Patel DJ, Fry DL: *In situ* pressure-radius-length measurements in ascending aorta of anesthetized dogs, *J. Appl. Physiology*, 19:413-426, 1964
17. Qiu Y, Tarbell JM: Numerical Simulation of pulsatile flow in compliant curved tube model of a coronary artery, *J. Biomech Eng*, 122:77 -85, 2000
18. Perktold K, Peter R, Resch M: Pulsatile non-Newtonian blood flow simulation through a bifurcation with an aneurysm. *Biorheology*, 26:1011-1030, 1989
19. Bederson JB, Awad IA, Wiebers DO, *et al.*: Recommendations for the management of patients with unruptured intracranial aneurysms: a statement for healthcare professional from Stroke Council of American Heart Association. *Stroke*, 31:2742-2750, 2000
20. Rosenorn J, Eskesen V: Patients with ruptured intracranial saccular aneurysms: clinical features and outcome according to the size, *Br J Neurosurg*, 8(1):73-8, 1994
21. Rosenorn J, Eskesen VN: Is there a connection between size and risk of bleeding in unruptured intracranial aneurysms? *Ugeskr Laeger*, 56(33):4704-7, 1994
22. Stehbens WE: Flow disturbances in glass models of aneurysms at low Reynolds numbers. *Quart. J Exp. Physiol*, 59: 167-174, 1974

23. Stehbens WE: Flow in glass models of arterial bifurcation and berry aneurysms at low Reynolds numbers. *Q J Exp. Physiol*, 60: 181-192, 1975
24. Stehbens WE: Etiology of intracranial berry aneurysms. *J Neurosurg*, 70:823-831, 1989
25. Stehbens WE: Ultrastructure of aneurysms. *Arch Neurol (Chicago)*, 32:789-807, 1975
26. Meyermann R, Yasargil MG: Ultrastructure studies of cerebral aneurysm and angiomas gained operatively. *Adv Neurol*, 20:557-567, 1978
27. Hassler O: Scanning electron microscopy of saccular intracranial aneurysms. *Am J Pathol*, 68:511-519, 1972
28. Strother CM, Graves VB, Rappe A: Aneurysm hemodynamics: An experimental study. *AJNR Am J Neuroradiol*, 13:1089-1095, 1992
29. Ferguson GG: Physical factors in the initiation, growth and rupture of human intracranial saccular aneurysms. *J Neurosurg*, 37:666-677, 1972
30. Imbesi S, Kerber C: Analysis of slipstream flow in a wide necked basilar artery aneurysm: Evaluation of potential treatment regimens, *AJNR Am J Neuroradiol*, 22:721-724, 2001
31. Canham PB, Ferguson GG: A mathematical model for mechanics of saccular aneurysm, *Neurosurgery*, 17:291-295, 1985
32. Aenis M, Stancampiano AP, Wakhloo AK, *et al.*: Modeling of Flow in a Straight Stented and Nonstented Side Wall Aneurysm Model, *J. Biomech. Eng*, 119:206-213, 1997
33. Ujiie H, Tachibana H, Hiramatsu O, *et al.*: Effects of size and shape (aspect ratio) on the hemodynamics of saccular aneurysm: a possible index for surgical treatment of intracranial aneurysms, *Neurosurgery*, 45:119-130, 1999

34. Ujiie H, Tamano Y, Sasaki K, Hori T: Is the aspect ratio a reliable index for predicting the rupture of a saccular aneurysm? *Neurosurgery*, 48(3):495-503, 2001
35. Kassell, N.F., Torner, J.C.: Size of Intracranial Aneurysms, *Neurosurgery*, 12(3):291-297, 1983
36. Crompton MR: Mechanism of growth and rupture in cerebral berry aneurysms. *Br Med J*, 5496:1138-42, 1966
37. Kumar BV, Naidu KB: Hemodynamics in aneurysm. *Computers and Biomedical Research*, 29:119-139. 1996
38. Liou TM, Chang WC, Liao CC: Experimental study of steady and pulsatile flows in cerebral aneurysm model of various sizes at branching site. *J Biomech Eng*, 119(3):325-32, 1997
39. Niimi H, Kawano Y, Sugiyama I: Structure of blood flow through a curved vessel with an aneurysm. *Biorheology*, 21:603-615, 1984
40. Kondo S, Hashimoto N, Kikuchi H, *et al.*: Cerebral Aneurysms Arising at Nonbranching Sites: An Experimental Study. *Stroke*, 28:398-404, 1997
41. Burleson A, Turitto V: Computer modeling of intracranial saccular and lateral aneurysms for the study of their hemodynamics, *Neurosurgery*, 37(4):774-784, 1995.
42. Liepsch D, Moravec S: Pulsatile flow of non-Newtonian fluid in distensible models of human arteries. *Biorheology*, 21(4):571-86, 1984
43. Karino T, Kwong HH, Goldsmith HL: Particle flow behaviour in models of branching vessels: I. Vortices in 90 degrees T-junctions. *Biorheology*, 16(3):231-48, 1979
44. Glagov S, Zarins C, Giddens DP, *et al.*: Hemodynamics and atherosclerosis: insights and perspectives gained from studies of human arteries. *Arch. Pathol. Lab. Med*, 112: 1018-31, 1988

45. Malek, AM., Alper SL, Izumo S: Hemodynamic Shear Stress and Its Role in Atherosclerosis, *JAMA*, 282(21):2035-2042, 1999
46. Awad IA, Barrow DL: Giant Intracranial Aneurysms, American Association of Neurological Surgeons, pp. 35, 1995
47. Foutrakis GN, Yonas H, Scwabassi RJ: Saccular aneurysm formation in curved and bifurcating arteries. *AJNR Am J Neuroradiol*, 20:1309-1317, 1999
48. Sekhar LN, Heros RC: Origin, Growth and Rupture of Saccular Aneurysms: A Review. *Neurosurgery*, 8(2):248-260, 1981
49. McCormick WF, Acosta-Rua GJ: The size of intracranial saccular aneurysms. An autopsy study. *J Neurosurg*, 33:422-427, 1997.
50. Forget TR Jr, Benitez R, Veznedaroglu E, *et al.*: A review of size and location of ruptured intracranial aneurysms. *Neurosurgery*, 49(6):1322-1326, 2001
51. Chyatte D, Bruno G, Desai S, *et al.*: Inflammation and intracranial aneurysms. *Neurosurgery*, 45(5):1137-46, 1999
52. Bruno G, Todor R, Lewis I, *et al.*: Vascular extracellular matrix remodeling in cerebral aneurysms. *J Neurosurg*, 89:431-440, 1998
53. Kim S, Singh M, Huang J *et al.*: Matrix Metalloproteinase-9 in cerebral aneurysms. *Neurosurgery*, 41(3):642-647, 1997
54. Cajander S, Hassler O: Enzymatic destruction of the elastic lamella at the mouth of cerebral berry aneurysms? An ultrastructural study with special regard to the elastic tissue. *Acta Neurol Scand*, 53:171-181, 1976
55. Fukuda S, Hashimoto N, Naritomi H, *et al.*: Prevention of rat cerebral aneurysm formation by inhibition of nitric oxide synthase. *Circulation*, 101:2532-2538, 2000

56. Inci S, Spetzler RF: Intracranial aneurysms and arterial hypertension: A review and hypothesis. *Surg Neurol*, 53:530-542, 2000
57. Stratos C, Stefanadis C, Kallikazatos I, *et al.*: Ascending aorta distensibility abnormalities in hypertensive patients and response to nifedipine administration. *Am J Med*, 93:505-512, 1992
58. Liou T, Liao C: Flowfields in lateral aneurysm models arising from parent vessels with different curvatures using PTV, *Experiments in Fluids*, 23:288-298 1997
59. Liou T, Liou S: A Review on *in vitro* studies of hemodynamic characteristics in terminal and lateral aneurysm models. *Proc. Natl. Sci. Counc ROC(B)*, 23(4):133-148, 1999
60. Rossitti S: Shear stress in cerebral arteries carrying saccular aneurysms. A preliminary study. *Acta Radiol*, 39(6):711-717, 1998
61. Kondo S, Hashimoto N, Kikuchi H, *et al.*: Cerebral aneurysms arising at nonbranching sites: an experimental study. *Stroke*, 28:398-404, 1997
62. Jackson ZS, Gotlieb AI, Langille BL: Wall tissue remodeling regulates longitudinal tension in arteries. *Circulation Research*, 90:918-925, 2002
63. Langille BL: Arterial remodeling: relation to hemodynamics. *Can J Physiol Pharmacol*, 74(7):834-41, 1996
64. Lehoux S, Tronc F, Tedgui A: Mechanisms of Blood Flow- Induced Vascular Enlargement. *Bioreheology*, 39(3-4): 319-24, 2002
65. Tronc F, Mallat Z, Lehoux S, *et al.*: A: Role of Matrix Metalloproteinases in Blood Flow-Induced Arterial Enlargement. *Arterioscler Thromb Vasc Biol*, 20:120-126, 2000
66. Tronc F, Wassef M, Esposito B, *et al.*: Role of NO in Flow-Induced Remodeling of the Rabbit Common Carotid Artery. *Arterioscler Thromb Vasc Biol*, 16:1256-1262, 1996

67. Masuda H, Zhuang YJ, Singh TM, *et al.*: Adaptive remodeling of internal elastic lamina and endothelial lining during flow -induced arterial enlargement. *Arterioscler Thromb Vasc Biol*, 19(10):2298-307, 1999
68. Butty VD, Gudjonsson, K, Buchel P, *et al.*: Residence times and basins of attraction for a realistic right internal carotid artery with two aneurysms. *Biorheology*, 39(3-4):387-93, 2002
69. Fry DL: Acute vascular endothelial changes associated with increased blood velocity gradients. *Circulation Research*, 22:165-197, 1968
70. Fry DL: Certain histological and chemical responses of the vascular interface to acutely induced mechanical stress in the aorta of the dog. *Circulation Research*, 14:93-108, 1969
71. Steiger HJ: Pathophysiology of Development and Rupture of Cerebral Aneurysm, *Acta Neurochirurgica Supplementum*, 48, 1990
72. Lehou S, Tronc F, Tedgui A: Mechanisms of blood flow-induced vascular enlargement. *Biorheology*, 39(3-4):319-324, 2002
73. Slack SM, Cui Y, Turitto VT: The effects of flow on blood coagulation and thrombosis. *Thrombosis and Haemostasis*, 70(1), 129-134, 1993
74. Singh TM, Zhuang YJ, Zarins CK, *et al.*: Reduction in wall shear stress below normal stimulates intimal thickening. *Cardiovascular Surgery*, 120, 1997
75. Szikora I, Wakhloo AK, Guterman LR, *et al.*: Initial experience with collagen-filled Guglielmi detachable coils for endovascular treatment of experimental aneurysms. *AJNR Am J Neuroradiol*, 8:667-672, 1997
76. Hadmenos GJ, Massoud TF: Biophysical mechanisms of stroke. *Stroke*, 28 (10):2067-2077, 1997

77. Amol Mulay, Computational modeling of cerebral aneurysm hemodynamics: effect of stenting, Master Thesis, State University of New York at Buffalo, USA, 2002.
78. Debrun GM, Aletich VA, Thornton J, *et al.*: Techniques of coiling cerebral aneurysms. *Surgical Neurology*, 53(2):150-156, 2000
79. Futami K, Yamashita J, Tachibana O, *et al.*: Basic fibroblast growth factor may repair experimental cerebral aneurysms in rats. *Stroke*, 26(9):1649-1654, 1995
80. Geremia G, Haklin M, Brennecke L: Embolization of experimentally created aneurysms with intravascular stent devices. *AJNR Am J Neuroradiol*, 15(7):1223-1231, 1994
81. Geremia G, Brack T, Brennecke L, *et al.*: Occlusion of experimentally created fusiform aneurysms with porous metallic stents. *AJNR Am J Neuroradiol*, 21(4):739-45, 2000
82. Wakhloo AK, Lanzino G, Lieber BB, *et al.*: Stents for intracranial aneurysms: the beginning of a new endovascular era? [Comment. Editorial] *Neurosurgery*, 43(2):377-379, 1998
83. Kwan ESK, Heilman CB, Shucart WA, *et al.*: Enlargement of basilar artery aneurysms following balloon occlusion – “water hammer effect” *J. Neurosurg*, 75:963-968, 1991.
84. Piotin, M, Mandai S, Murphy KJ, *et al.*: Dense Packing of Cerebral Aneurysms: An *In vitro* Study with Detachable Platinum Coils, *AJNR Am J Neuroradiol*, 21:757-760, 2002
85. Ortega H: Computer simulation helps predict cerebral aneurysm, Journal articles by Fluent Software users, JA071, 1999
86. Masuda H, Bassiouny H, Glagov S, *et al.*: Artery wall restructuring in response to increased flow. *Surg Forum*, 40:285-286, 1989

87. Arnal JF, Dinh-Xuan AT, Darblade B, *et al.*: Endothelial NO synthase in physiology and pathology. *Cellular and Molecular Life Sciences*, 1078-1087, 1999
88. Kamiya A, Togawa T: Adaptive regulation of wall shear stress to flow change in the canine carotid artery. *American Journal of Physiology*, 239, H14-H21, 1980
89. Guzman RJ, Abe K, Zarins CK: Flow-induced arterial enlargement is inhibited by suppression of nitric oxide synthase activity *in vivo*. *Surgery*, 122:273-280, 1997
90. Ku D: Blood flow in arteries, *Annual Review of Fluid Mechanics*, 29:399-434, 1997
91. Tateshima S, Murayama Y, Villablanca JP, *et al.*: Intraaneurysmal flow dynamics study featuring an acrylic aneurysm model manufactured using a computerized tomography angiogram as a mold. *J Neurosurg*, 95:1020-1027, 2001
92. Tateshima S, Murayama Y, Gobin YP, *et al.*: Endovascular treatment of basilar tip aneurysms using Guglielmi detachable coils: anatomic and clinical outcomes in 73 patients from a single institute, *Neurosurgery*, 47(6):332-342, 2000
93. Murayama Y, Song JK, Uda K: Combined endovascular treatment for both intracranial aneurysm and symptomatic vasospasm., *AJNR Am J Neuroradiol*, 24(1):133-139, 2003
94. Zubillaga AF, Guglielmi G, Vinuela F, *et al.*: Endovascular occlusion of intracranial aneurysm with electrically detachable coils: Correlation of aneurysm neck size and treatment results, *AJNR Am J Neuroradiol*, 15:815-820, 1994
95. Turjman F, Massoud TF, Sayre J, *et al.*: Predictors of aneurysmal occlusion in the period immediately after endovascular treatment with detachable coils: a multivariate analysis, *AJNR Am J Neuroradiol*, 19:1645-1651, 1998
96. Albuquerque FC, Spetzler, RF, Zabramski JM, *et al.*: Effects of Three-dimensional Angiography on the Coiling of Cerebral Aneurysms. *Neurosurgery*, 51(3):597-606, 2002

97. Graves VB, Strother CM, Partington, *et al.*: Flow dynamics of lateral carotid artery aneurysms and their effects on coils and balloons: An experimental study in Dogs, *AJNR Am J Neuroradiol*, 13:189-196, 1992
98. Rosenorn J, Eskensen V: Does a safe size-limit exist for unruptured intracranial aneurysms? *Acta Neurochir (Wien)*, 121: 113–118, 1993
99. Butty VD, Gudjonsson K, Buchel P, *et al.*: Residence times and basins of attraction for a realistic right internal carotid artery with two aneurysms. *Biorheology*, 39(3-4):387-93, 2002
100. Cebral JR, Löhner R, Burgess J: Computer Simulation of Cerebral Artery Clipping: Relevance to Aneurysm Neuro-Surgery Planning, *Proc. ECCOMAS*, Sep. 11-14, Barcelona-Spain, 2000
101. Vorp D, Steinman D, Ethier CR: Computational Modeling of arterial biomechanics, *Comput Sci Eng*, 3(5):51-62, Sept/Oct, 2001
102. Steinman DA, Milner JS, Norley CJ, *et al.*: Image-based computational simulation of flow dynamics in a giant intracranial aneurysm. *AJNR Am J Neuroradiol*, 24(4):559-566, 2003
103. Andow J, Kamiya A: Blood flow and vascular endothelial cell function. *Front Med Biol Eng*, 5:245-264, 1993
104. Zarins CK, Zatina MA, Giddens DP, *et al.*: Shear stress regulation of artery lumen diameter in experimental atherogenesis. *J Vasc Surg*, 5(3):413-420 1987
105. Masuda H, Zhuang YJ, Singh TM, *et al.*: Adaptive remodeling of internal elastic lamina and endothelial lining during flow-induced arterial enlargement. *Arterioscler Thromb Vasc Biol*, 19(10):2298-307 1999

106. Rogers L: Intracranial aneurysm size and potential for rupture (Letter). *J Neurosurg*, 67:475-476, 1987
107. Schievink WI, Piepgras DG, Wirth FP: Rupture of previously documented small asymptomatic saccular intracranial aneurysms. Report of three cases. *J Neurosurg*, 76:1019-1024, 1992
108. Bederson JB, Awad IA, Wiebers DO, *et al.*: Recommendations for the management of patients with unruptured intracranial aneurysms: a statement for healthcare professionals from Stroke Council of the American Heart Association. *Stroke*, 31:2742-2740, 2000
109. Gobin YP, Counord JL, Flaud P, *et al.*: *In vitro* study of haemodynamics in a giant saccular aneurysm model: influence of flow dynamics in the parent vessel and effects of coil embolisation. *Neuroradiology*, 36(7):530-536, 1994
110. Hashimoto N, Kim C, Kikuchi H, *et al.*: Experimental induction of cerebral aneurysms in monkeys. *J Neurosurg*, 67:903-905, 1987
111. Long Q, Xu XY, Collins MW, *et al.*: The combination of magnetic resonance angiography and computational fluid dynamics: a critical review. *Critical Reviews in Biomedical Engineering*, 26(4):227-274, 1998
112. Davies PF, Tripathi SC: Mechanical Stress mechanisms and the cell: an endothelial paradigm. (mini review) *Circulation Research*, 72:239-245, 1993
113. Hoffmann, KR, Sen A, Lan L, *et al.*: A system for determination of 3D vessel tree centerlines from biplane images. *International Journal of Cardiac Imaging*, 16:315-330, 2000
114. Hoffmann KR, Wahle A, Barakat CP: Biplane X-ray angiograms, intravascular ultrasound and 3D visualization of coronary vessels. *International Journal of Cardiac Imaging*, 15:495-512, 1999

115. Alperin A, Hoffmann KR, Doi K: Automated extraction of vasculature information from angiographic images using a vessel tracking algorithm. In Chen CT, editor. Medical imaging 1396. *Proceeding of the Midwest Chapter of the Society of Photo-instrumentation and Engineering, Chicago, IL SPIE*, pp.27-31, 1991
116. Sen A, Lan L, Doi K, *et al.*: Quantitative evaluation of a coronary vessel tracking technique on clinical angiographic projections. *Med Phys*, 26:698-706, 1999
117. Schoeneman PH: A generalized solution of the orthogonal Procrustes problem. *Psychometrika*, 31:1-10, 1996
118. Neil-Dwyer G, Barlett JR, Nicholls AC, *et al.*: Collagen deficiency and ruptured cerebral aneurysms: A clinical and biochemical study. *J Neurosurg*, 59:16-20, 1983
119. Ostergaard JR, Oxlund H: Collagen type III deficiency in patients with rupture of intracranial saccular aneurysms. *J Neurosurg*, 67:690-696, 1987
120. Norrgard O, Angquist KA, Fodstad H, *et al.*: Intracranial aneurysms and heredity. *Neurosurgery*, 20:236-239, 1987